Chemical Geology 641 (2023) 121772

Contents lists available at ScienceDirect

Chemical Geology

journal homepage: www.elsevier.com/locate/chemgeo

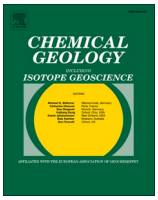

The Singhbhum Craton (India) records a billion year of continental crust formation and modification

Sukalpa Chatterjee [a,*], Klaus Mezger [a], Om Prakash Pandey [b], Melanie Kielman-Schmitt [c], Alina Hofer [a], Ellen Kooijman [c]

[a] Institut für Geologie, Universität Bern, Bern, Switzerland
[b] Department of Earth Sciences and Engineering, King Abdullah University of Science and Technology (KAUST), Thuwal, Saudi Arabia
[c] Department of Geosciences, Swedish Museum of Natural History, Stockholm, Sweden

ARTICLE INFO

Editor: Dr. S Aulbach

Keywords:
Continental crust
Paleoarchean
Singhbhum Craton
Sr-isotopes in apatite
Genesis of TTG suite

ABSTRACT

The petrogenesis of continental crust from its ultimate mantle source can be reconstructed from the element abundances and radiogenic isotope compositions of ideally pristine igneous rocks. The initial isotope compositions of igneous rocks provide geochemical constraints on the age, composition and evolution of their source(s). Determining initial isotope ratios for rock samples can be challenging, especially in rocks with a long and protracted thermal history. The Rb-Sr system is highly sensitive to parent-daughter element fractionation during magma differentiation. This makes the Rb-Sr isotope systematics ideal to trace the precursor composition of Archean felsic crust and constrain the time of element fractionation during the formation and subsequent modification of continental crust. Initial isotope compositions can be obtained directly from minerals that strongly prefer the daughter element and effectively exclude the parent element of the radio-isotope system of interest. Apatite, having a near zero Rb/Sr ratio, is ideal for preserving its initial $^{87}Sr/^{86}Sr$ and zircon records initial $^{176}Hf/^{177}Hf$ compositions. Combined modelling of Sr and Hf isotope data from granitoids of the Archean Singhbhum Craton, indicates that the older Paleoarchean granitoids, emplaced between 3.53 Ga and 3.44 Ga, were derived from a mafic precursor (~52–54 wt% SiO_2) sourced from a depleted mantle at ~3.71 Ga. Initial $^{87}Sr/^{86}Sr$ isotope signatures of matrix apatite and apatite inclusions in zircon from the younger Paleoarchean granitoids (3.4–3.2 Ga) of the Singhbhum Craton indicate these younger granitoids were produced by mixing of magma generated from an older mafic source and partial melts derived from the older granitoids. The combined Sr-Hf isotope modelling links the timing of mantle extraction of the precursor material for Paleoarchean Singhbhum granitoids with a known mafic crust extraction event at ~3.71 Ga. In combination, the new Sr isotope data from apatite combined with whole rock and zircon Hf isotope data from the literature reveal a ~1 Ga protracted crustal growth and differentiation history of the nucleus of the Singhbhum Craton. By combining radio-isotope systems like ^{87}Rb-^{87}Sr and ^{176}Lu-^{176}Hf, the petrogenesis of Archean felsic crust from the extraction of mafic material from the mantle to reworking in an orogenic cycle to emplacement can be reconstructed. This approach can be applied to other greenstone-gneiss terranes to quantify the spatio-temporal and compositional evolution of voluminous felsic crust and the formation of cratons in the Archean.

1. Introduction

Among the rocky planets of the solar system, a unique characteristic of Earth is the presence of stable felsic continental landmass. Through time, changes in heat production, mantle dynamics, tectonics and crust mantle differentiation processes have led to the extraction of incompatible elements from the mantle, giving rise to the continental landmass and an increase in its volume.

Reconstructing the temporal and compositional evolution of source materials of Archean felsic crust is the key to reveal Hadean and Eoarchean crust formation and its subsequent evolution (Dhuime et al., 2015; O'Neil and Carlson, 2017; Emo et al., 2018). There is significant understanding of how the present-day subduction-driven plate tectonic mechanism works (Conrad and Lithgow-Bertelloni, 2002) and drives

* Corresponding author.
E-mail address: sukalpa.chatterjee@unibe.ch (S. Chatterjee).

https://doi.org/10.1016/j.chemgeo.2023.121772
Received 24 July 2023; Received in revised form 4 October 2023; Accepted 5 October 2023
Available online 12 October 2023

crust formation in arc regions (e.g. Jagoutz and Kelemen, 2015). However, exactly when plate tectonics started on Earth (Cawood et al., 2018; Stern, 2018 and references therein), and if not in its present style, what kind of tectonic processes fuelled continental crust formation in the Archean, is debated (e.g. Moyen, 2011; Moore and Webb, 2013; Sizova et al., 2015; Chowdhury et al., 2017; Moyen and Laurent, 2018; Hastie et al., 2023). This is mostly owing to the fact that preserved Paleoarchean and older rock records on Earth are extremely rare and with some exception (e.g. Kröner et al., 2013) there is no preservation of precursor materials for the Paleoarchean felsic crust. In addition, some of the key rock types and rock associations of the Hadean and Archean (tonalite-trondhjemite-granodiorite (TTG), komatiite) are only restricted to that time, and with very few exceptions, have not been produced after the Archean eon. Hence, some key questions remain unanswered about the nature of the earliest crust, the age of its mantle extraction, the composition and evolution of the precursor material and rate of crust extraction, which led to the formation of Archean felsic crust.

Robust information on the timing and extent of crust generation can be derived using radio-isotope systems that record the extent of parent/daughter element fractionation and its timing. Crustal differentiation leads to a much stronger fractionation of Rb/Sr than Lu/Hf and Sm/Nd. Typical parent daughter ratios in differentiated crustal rocks range only from ~0.009 to ~0.022 for $^{176}Lu/^{177}Hf$, and from ~0.10 to ~0.22 for $^{147}Sm/^{144}Nd$ (Boehnke et al., 2018; Gillespie et al., 2021a). In contrast $^{87}Rb/^{86}Sr$ ranges from ~0.05 in mafic rocks to well above 4 in felsic rocks, making this isotope system a highly sensitive tracer of magmatic differentiation. In addition, the Rb/Sr varies much more systematically with the SiO_2 content of rocks than Lu/Hf or Sm/Nd, making it ideal to track the time integrated compositional evolution of precursor material for Archean crust (Dhuime et al., 2015; Boehnke et al., 2018). The main obstacle in using Sr isotopes for petrogenetic studies of Archean felsic crust has been the difficulty to obtain initial $^{87}Sr/^{86}Sr$ for rocks, which is mostly due to the high $^{87}Rb/^{86}Sr$ in differentiated crustal materials. Initial $^{87}Sr/^{86}Sr$ ($^{87}Sr/^{86}Sr_{i)}$ is obtained from an isochron defined by a co-genetic suite of rocks or by back-calculation of the measured $^{87}Sr/^{86}Sr$ of a rock of well-known age. Using these approaches to obtain accurate and precise $^{87}Sr/^{86}Sr_i$ is difficult due to the susceptibility of Rb/Sr to post-emplacement modification by metamorphic overprinting and alteration (Page and Bell, 1986). This is particularly relevant in Archean terranes, which commonly have gone through multiple generations of tectonic and metamorphic events. Obtaining $^{87}Sr/^{86}Sr_i$ is also possible by direct measurement of primary minerals with near zero Rb/Sr, such as apatite. Recent studies of matrix apatite and apatite inclusions in zircon (Bruand et al., 2016; Antoine et al., 2020) from igneous rocks have shown that apatite can effectively preserve primary magmatic signatures. Apatite has also very low Rb/Sr resulting in significantly reduced radiogenic ^{87}Sr production, making it ideal to obtain $^{87}Sr/^{86}Sr_i$ by direct measurement. Advancements in LA-MC-ICPMS (Emo et al., 2018; Ravindran et al., 2020; Caton et al., 2022) and Secondary-Ion Mass Spectrometry (SIMS) (Gillespie et al., 2021a; Jeon and Whitehouse, 2021; Gillespie et al., 2021b) now enable precise measurements of $^{87}Sr/^{86}Sr$ in both matrix apatite and apatite inclusions in zircon.

Using whole rock-mica Rb-Sr ages and $^{87}Sr/^{86}Sr_i$ from matrix apatite and apatite inclusions in zircon from Paleoarchean granitoids, this study provides constraints on the composition and temporal evolution of the source(s) of the Paleoarchean felsic crustal nuclei of the Singhbhum Craton. For an efficient use of this system, it is essential to evaluate the preservation potential of $^{87}Sr/^{86}Sr_i$ composition in these felsic units, at the whole-rock as well as mineral scale, particularly in apatite. Cherniak and Ryerson (1993) and Cherniak (2000) determined relevant parameters for Sr diffusion in apatite, results of which indicate that ~250 μm apatite grains will retain primary Sr isotope signatures in lower amphibolite facies condition (~ 500 °C) even after 100 Myr of continuous metamorphism. Hence, the primary Sr isotope preservation potential is significant in large matrix apatite grains and apatite inclusions in robust phases like zircon. As there is a chance of resetting of the Sr isotopes in apatite, it is necessary to establish the time when the Sr isotope system in rocks and minerals could have been modified following rock emplacement or primary crystallization. Whole rock-mica Rb-Sr isochron ages were determined for different felsic units to determine the time of metamorphic overprinting across the craton. This was followed by, studying $^{87}Sr/^{86}Sr_i$ in matrix apatite and apatite inclusions in zircon from these felsic units to understand time integrated Sr isotope evolution of the Singhbhum Craton during the Paleoarchean. Furthermore, combined Sr and Hf isotope modelling (Supplementary Text- Section. 4) has been carried out using time integrated $^{87}Sr/^{86}Sr_i$ data from apatite and literature Hf_i data from whole rock samples and in-situ zircon studies on the same Paleoarchean felsic units (Pandey et al., 2019; Upadhyay et al., 2019). This modelling approach of combining isotope systems with very different geochemical behaviour during differentiation yields information on the extraction and formation of different source materials along with their time-integrated evolution, which led to the formation of extensive Archean felsic crust in the Singhbhum Craton.

2. Geological background

The Singhbhum Craton is exposed across ~40,000 km^2 in eastern India (Fig. 1) and is one of the most pristine Archean cratons preserved on Earth with voluminous felsic crust dominated by TTGs and granites, which are predominantly of Paleoarchean to Mesoarchean (3.6–3.05 Ga) age. The oldest xenocrystic zircon crystal found so far is 4.24 Ga old (Chaudhuri et al., 2018), suggesting the presence of some older, albeit possibly minor, evolved crustal material. The exposed Paleoarchean rocks include members of the TTG suite and granites (Fig. 1) (Saha, 1994; Upadhyay et al., 2014; Dey et al., 2017; Mitra et al., 2019; Pandey et al., 2019; Upadhyay et al., 2019; Chaudhuri et al., 2022; Hofmann et al., 2022) and greenstone belts which flank the felsic nucleus in the eastern, western and southern part of the craton (Fig. 1) (Saha, 1994; Mukhopadhyay et al., 2008). The greenstone belts contain dominantly mafic-ultramafic volcanic rocks as well as clastic (meta-pelites) and chemical sediments (banded iron formation, chert) with minor intermediate and felsic components (Mukhopadhyay et al., 2008; Jodder et al., 2023, 2021). The minor felsic components present within the Daitari Greenstone Belt (formerly known as Southern Iron Ore Group) and the Gorumahisani Greenstone Belt (formerly known as Eastern Iron Ore Group) are all ~3.51 Ga old (Mukhopadhyay et al., 2008; Jodder et al., 2021, 2023).

One of the oldest lithological units in the craton is the Older Metamorphic Group (OMG), which has recently been described as the high grade metamorphosed westward extension of the Badampahar Group (Hofmann et al., 2022) of Gorumahisani Greenstone Belt. It includes metasedimentary schists interlayered with amphibolites preserved as enclaves within the Singhbhum Granite (Mukhopadhyay and Matin, 2020). The $^{207}Pb/^{206}Pb$ detrital zircon and whole-rock Sm-Nd ages from the OMG range from 3.6 Ga (Goswami et al., 1995; Mishra et al., 1999) to 3.3 Ga (Sharma et al., 1994). This unit was deposited at ~3.37 Ga in a supra-subduction zone setting (Mukhopadhyay and Matin, 2020), although Goswami et al. (1995), suggested a ~3.5 Ga sedimentation age for this unit.

Members of the TTG suite and granites constitute most of the cratonic nucleus. The TTGs are grouped under Champua Suite (Dey et al., 2017; Hofmann et al., 2022) (also known as Older Metamorphic Tonalite Gneiss), whereas multiple phases of Singhbhum Granites and several granitic bodies like the Bonai granite, Mayurbhanj granite, Chakradharpur granite, and Pallahara gneiss (Fig. 1) represent the granitic part (Dey et al., 2019; Mukhopadhyay and Matin, 2020; Chaudhuri, 2020; Chaudhuri et al., 2022; Hofmann et al., 2022). Multiple phases of Singhbhum Granites have been grouped into the Singhbhum Suite (Dey et al., 2017; Hofmann et al., 2022). The Champua Suite rocks are mostly metamorphosed to greenschist to amphibolite

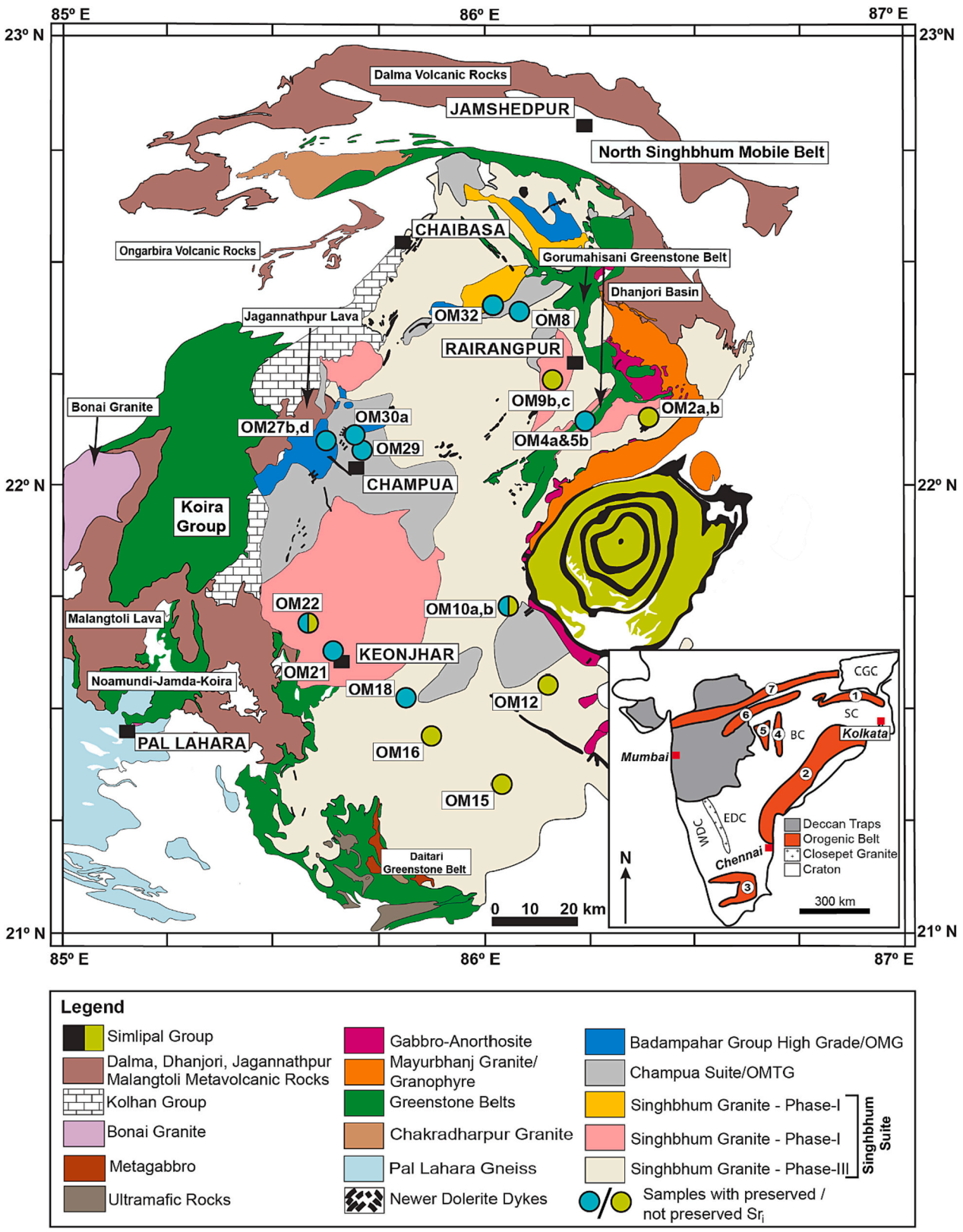

Fig. 1. Simplified geological map of Singhbhum Craton (modified after Saha, 1994; Pandey et al., 2019) with sample locations. Orogenic belts: (1) NSMB - North Singhbhum Mobile Belt; (2) Eastern Ghats; (3) Pandyan; (4) Dongargarh; (5) Sakoli; (6) Satpura: (7) CITZ - Central Indian Tectonic Zone; BC - Bundelkhand Craton; WDC - Western Dharwar Craton; EDC - Eastern Dharwar Craton; SC - Singhbhum Craton; BC - Bastar Craton; CGC - Chhotanagpur Gneiss Complex. (For interpretation of the references to colour in this figure legend, the reader is referred to the web version of this article).

facies and are found as enclaves within the Singhbhum Suite (Fig. 1). U-Pb zircon ages of the Champua Suite show two distinct clusters of 3.53–3.44 Ga and 3.35–3.32 Ga (Mishra et al., 1999; Acharyya et al., 2010; Upadhyay et al., 2014). Whole-rock εNd_i values of the Champua Suite are positive (+0.11 to +1.7, Sharma et al., 1994; +0.5 to +4.5, Pandey et al., 2019; +0.1 to +2.4, Upadhyay et al., 2019). Similarly whole-rock and in-situ zircon εHf_i values are also positive (+2.1 to +4.8, Dey et al., 2017; +0.6 to +1, Pandey et al., 2019; +0.7 to +4.3, Upadhyay et al., 2019; +1.3 to +4.1 for Kalikapur Diorite gneiss, +0.3 to +3.4 for Bisoi tonalite, 0 to +2.2 for Rairangpur trondhjemite, Mitra et al., 2022). The Singhbhum Suite is composed of plutons formed by multiple granitic intrusions between 3.4 and 3.2 Ga with progressively lower εNd_i and εHf_i values for the younger granites (Dey et al., 2019; Mitra et al., 2019; Upadhyay et al., 2019; Pandey et al., 2019; Mitra et al., 2022). The emplacement of Singhbhum Suite of granites was contemporaneous with high-grade metamorphism of the Champua Suite and the high-grade overprinting of westward extension of Badampahar group (OMGs) at ~3.3–3.2 Ga (Prabhakar and Bhattacharya, 2013; Upadhyay et al., 2014).

3. Methods

For this study, a total of 19 rock samples were selected. Within them, 18 samples are TTGs, granites and paragneisses from the Champua Suite, Singhbhum Suite and high grade equivalent of the Badampahar Group (OMG) [Fig. 1, Supplementary Table (ST-1)]. One sample, selected from the study of Pandey et al. (2019) (Fig. 1, ST-1) is a basaltic andesite from the Badampahar Group of the Gorumahisani Greenstone Belt (Jodder et al., 2021). Samples were screened for apatite, zircon and mica after the samples had been crushed in a jaw-crusher and comminuted in a disc mill, followed by sieving to obtain the <500 μm fraction. This fraction was then passed through a magnetic separator. Mica was handpicked from the magnetic fraction. The non-magnetic fraction was passed through heavy liquid (CH_3I). The density of the heavy liquid was modified by diluting with acetone to separate zircon and apatite simultaneously. Subsequently zircon and apatite were handpicked from each sample. Strontium isotopes were measured in apatite from 18 samples. In 13 of these samples, zircon crystals were found with apatite inclusions, which were also analysed. In addition, five samples (four of them from the batch of 18 samples mentioned above and one additional) were selected for Rb-Sr dating using mica-whole rock pairs (ST-1).

3.1. Mica $^{87}Sr/^{86}Sr$

Separated mica fractions were gently ground in an agate mortar with acetone to separate possible inclusions of feldspar and apatite, which were later removed by sieving with a 150 μm mesh nylon fabric. The mica residue was cleaned with ethanol and ~10–20 mg of mica was collected from each sample. All six samples were spiked with an enriched ^{87}Rb-^{84}Sr tracer and digested in 40% HF for 48 h on a hotplate at 120 °C. Subsequently, they were dried at 100 °C and re-dissolved in 14 M HNO_3 and 11 M HCl at 110 °C in two subsequent steps, with a drying step in between at 100 °C. Following complete dissolution, Rb and Sr were separated from sample matrix on a 5 cm long Dowex 50 W-X8 cation exchange resin column. Rubidium was eluted with 4 ml 2.5 M HCl, followed by elution of Sr with 8 ml of 2.5 M HCl. Rb isotopes were measured on a Thermo Scientific™ Neptune Plus™ MC-ICP-MS and the Sr isotope composition was measured on Thermo Scientific™ Triton Plus™ Thermal Ionization Mass Spectrometer (TIMS), at the Institute of Geological Sciences, University of Bern, Switzerland. Rb isotope ratios were corrected for mass bias using the JMC Rb solution standard by sample-standard bracketing. For Sr isotope analysis, Sr cuts were loaded in 6.4 M HCl on degassed rhenium single filaments with Ta-fluoride activator. The exponential law and an iteration method (Stracke et al., 2013) were used to correct for instrumental mass bias. NIST SRM® 987 was used as external standard during Sr isotope measurements. All ratios were corrected for instrumental mass fractionation using $^{86}Sr/^{88}Sr = 0.1194$. NIST SRM® 987 yielded an average $^{87}Sr/^{86}Sr = 0.710346$ (14) (2SE; $n = 13$) during the measurement session. BCR-2 was measured as the whole rock standard and during measurement yielded $^{87}Sr/^{86}Sr = 0.704985(9)$. All samples were adjusted for the offset of the BCR-2 measured value from the literature value of $^{87}Sr/^{86}Sr = 0.704958(6)$ (Raczek et al., 2003). Isochrons were obtained using the Rb-Sr systematics of the mica separates given in Table 1 and the whole-rock data in Pandey et al. (2019).

3.2. Apatite $^{87}Sr/^{86}Sr$

3.2.1. Sample preparation

With the aim of measuring matrix apatite and apatite inclusions in zircon, both apatite and zircon crystals were picked from the heavy liquid separate fraction. Care was taken to select apatite crystals without any visible inclusions, whereas for zircon, crystals with the highest number of inclusions were targeted. Two separate epoxy mounts were prepared for matrix apatite and zircon. The apatite mount was polished approximately to the centre of the apatite grains, whereas the zircon mount was polished to expose most inclusions at the surface. Both mounts were studied using backscattered electron (BSE) and cathodoluminescence (CL) imaging along with energy-dispersive X-ray spectroscopy (EDS) on a ZEISS EVO50 SEM at the Institute of Geological Sciences, University of Bern, Switzerland. BSE imaging (Figs. 2 & 3) and EDS spectra were used to find and characterize mineral inclusions within both matrix apatite and zircon grains. Along with SEM imaging, both transparent epoxy mounts were also studied under transmitted light with an Olympus BX51 microscope.

3.2.2. Apatite $^{87}Sr/^{86}Sr$ analysis

The $^{87}Sr/^{86}Sr$ composition of both matrix apatite grains and apatite inclusions in zircon was analysed in-situ on a Nu plasma (II) MC-ICPMS connected to an ESI NWR193 ArF excimer laser ablation system, housed at the Vegacenter, Swedish Museum of Natural History, Stockholm. Data were acquired following the method outlined in Emo et al. (2018). Depending on the selected area in the matrix apatite grains, spots ranging from 50 to 90 μm in diameter were analysed (Fig. 2). For apatite inclusions in zircon, 20 and 30 μm circular spots were used along with 15 × 35 μm, 15 × 50 μm, 40 × 70 μm (Fig. 2f) rectangular spots, which are volumetrically equal to 26 μm, 30 μm and 60 μm circular spot sizes, respectively. Other rectangular spot sizes including 22 × 33 μm, 22 × 40 μm and 15 × 45 μm were also used while measuring the apatite inclusions within zircon. Rectangular spots were used, because many inclusions are exposed parallel to their c-axis, and hence had a rectangular exposed surface (Fig. 3a & 3b).

During analysis, laser fluence was kept at 2.6 J/cm^2 with a repetition rate of 15 Hz. The sample ablation time was 35 s, with 40 s of washout and baseline measurement before each ablation. Longer baseline measurements are needed to properly correct for the $^{86,84,82}Kr^+$ isobaric

Table 1
Initial $^{86}Sr/^{87}Sr$ of apatite from the Paleoarchean rocks from the Singhbhum Craton.

Sample	$^{87}Sr/^{86}Sr_i$	2SE	Age (Ga)
OM-4a	0.70078	0.00006	3.262
OM-5b	0.70112	0.00027	3.335
OM-8 + OM-10a	0.70029	0.00063	3.440
OM-18	0.70163	0.00038	3.292
OM-21	0.70105	0.00043	3.320
OM-22	0.70102	0.00051	3.327
OM-29	0.70070	0.00030	3.363
OM-30a	0.70086	0.00005	3.320
OM-32	0.70148	0.00015	3.320

External 2SE of the samples are reported here in the table. Reference for the ages of individual samples can be found in Supplementary Table ST-6.

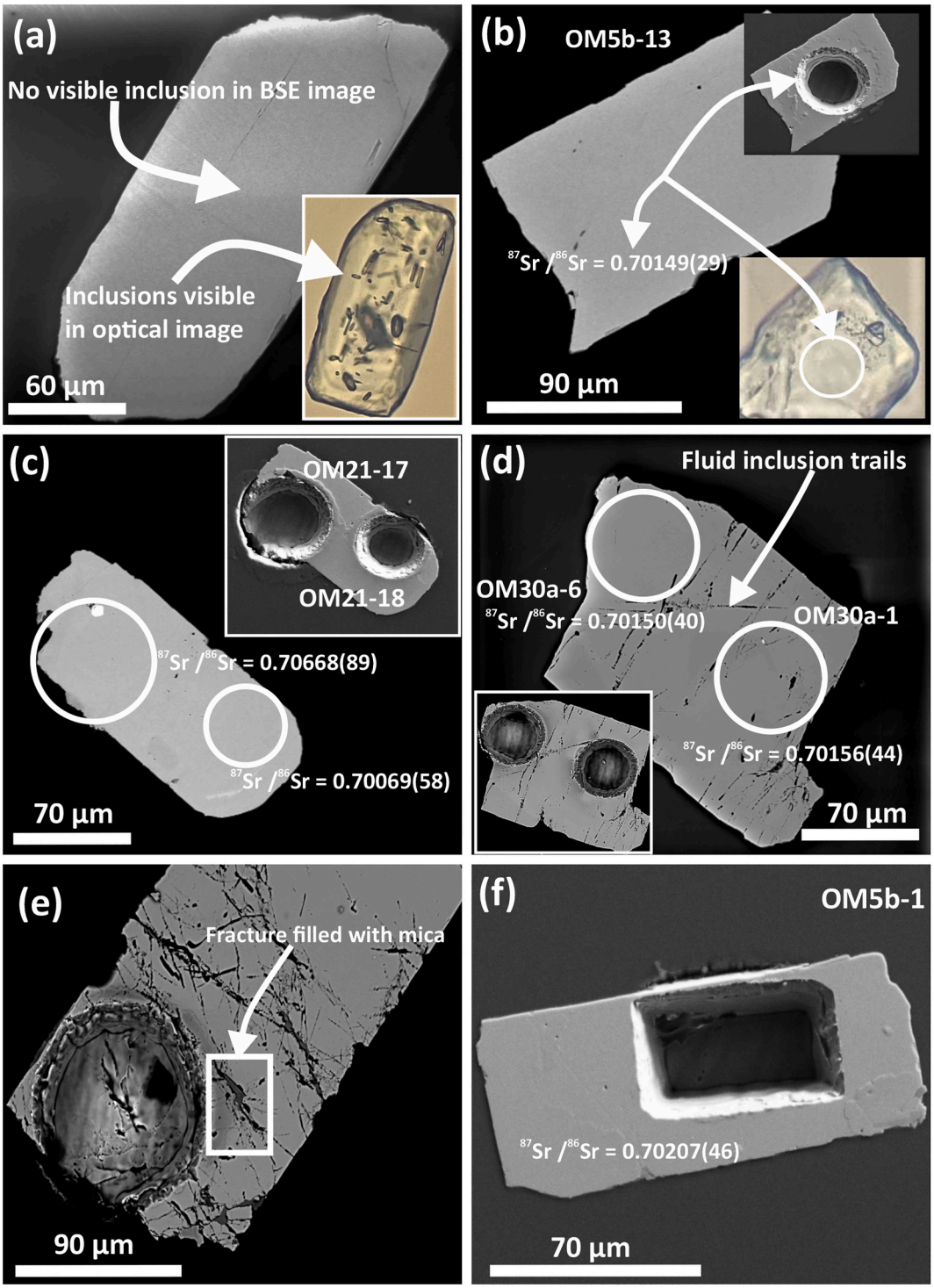

Fig. 2. Back Scattered Electron (BSE) and optical images of matrix apatite grains. (a)-(b) Illustrating the importance of combining optical and BSE imaging to select laser ablation spots to avoid ablation of hidden inclusions. (c) Ablation of mineral inclusions (spot OM21–17) in apatite increases $^{87}Sr/^{86}Sr$ by ~8.5‰ compared to pure apatite (spot OM21–18), (d) Inclusion trails, (e) Fractures within a matrix apatite grain filled with mica, (f) 70 × 30 µm laser ablation pit in matrix apatite exposed parallel to its c-axis, giving similar precision (2SE) as commonly used circular spots.

interferences, as Kr is introduced into the system with the Ar gas. All potential isobaric interferences on different Rb and Sr isotope masses and cup configuration for the measurements are provided in ST-2. After analysis, corrections were done offline using a custom DRS (data reduction scheme) for Iolite v2.5. First isobaric interferences of Kr^{+} were removed by on-peak baseline subtraction, followed by different REE^{2+} interference corrections. Er^{2+} and Yb^{2+} interference on different Rb and Sr isotopes were corrected using measured $^{166}Er^{2+}$ m/z on mass 83 (on L2 cup) and interference-free $^{171}Yb^{2+}$ and $^{173}Yb^{2+}$ half masses on mass 85.5 and 86.5 at cup H3 and cup H5, respectively, along with the natural ratios of $^{164}Dy/^{163}Dy = 1.13173$, $^{164}Er/^{166}Er = 0.047873$, $^{168}Er/^{166}Er = 0.797084$, $^{170}Er/^{166}Er = 0.44421$, $^{172}Yb/^{173}Yb = 1.353378$, $^{174}Yb/^{173}Yb = 1.97334$, $^{176}Yb/^{173}Yb = 0.79107$. Following REE^{2+}, interference corrections for Ca-argides and Ca-dimers were made by measuring

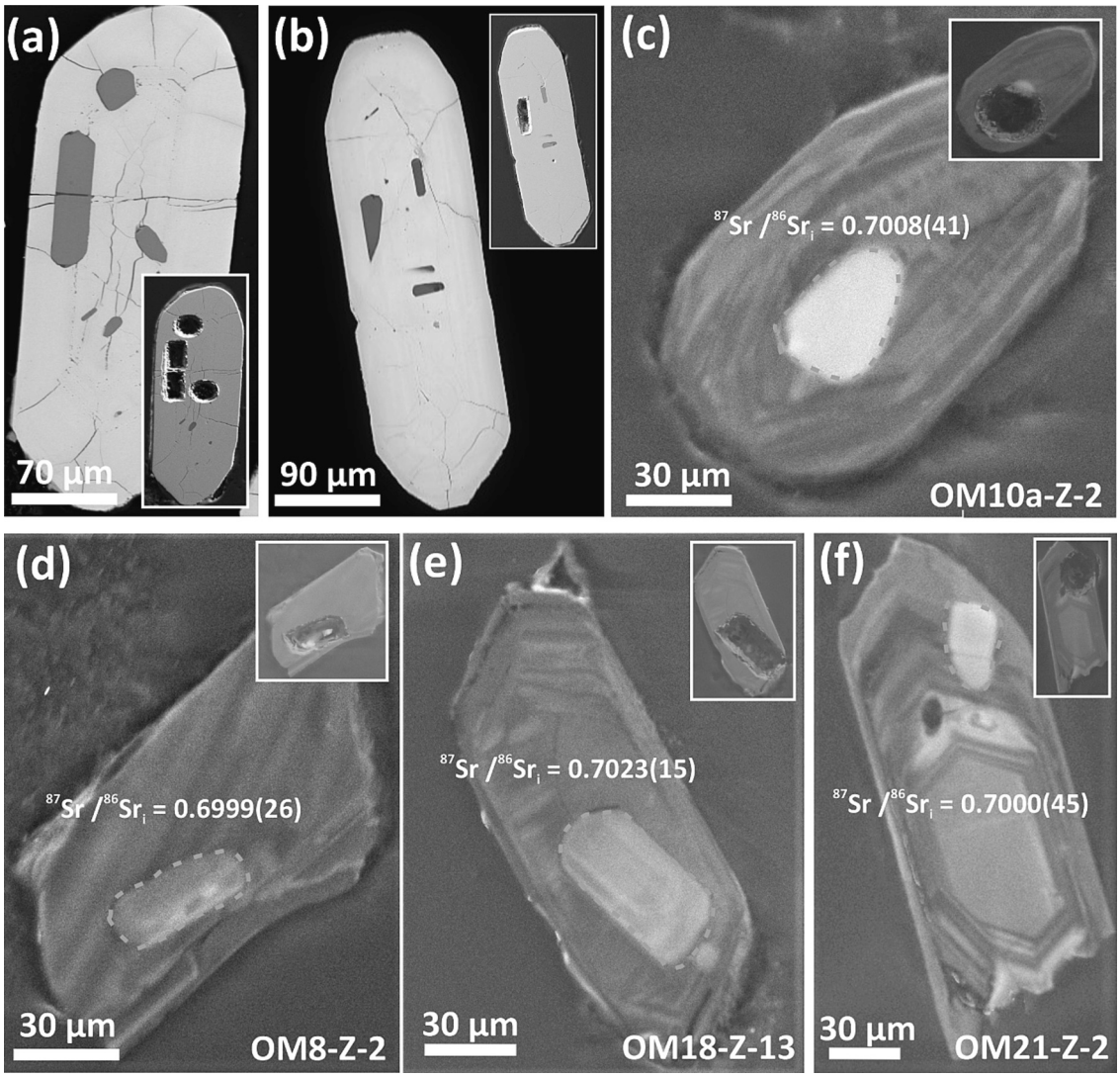

Fig. 3. Back Scattered Electron (BSE) and Cathodoluminescence (CL) images of zircons containing apatite inclusions. (a)-(b) presence of multiple large apatite inclusions measurable by LA-MC-ICPMS. Both apatite inclusions parallel and perpendicular to c-axis are exposed. Fractures cutting through and reaching up to apatite inclusions can increase open system behaviour and can contain high-Rb minerals. (c)-(f) Age corrected initial $^{87}Sr/^{86}Sr$ of best preserved enclosed apatite grains.

$^{40}(CaAr)^{42}Ca$ (on mass 82; cup L4) signal (which is considered to be the residual after correcting for $^{82}Kr^{+}$, $^{164}Er^{2+}$ and $^{163}Dy^{2+}$ signals on mass 82) and using the natural abundance ratios of $^{40}(CaAr)^{43}Ca/^{40}(CaAr)^{42}Ca$ = 0.20865, $^{40}(CaAr)^{44}Ca/^{40}(CaAr)^{42}Ca$ = 3.22410 and $^{40}(CaAr)^{48}Ca/^{40}(CaAr)^{42}Ca = 0.2890$. Mass bias of Sr was corrected using natural $^{86}Sr/^{88}Sr$ = 0.1194 and exponential fractionation law. $^{87}Rb^{+}$ interference on $^{87}Sr^{+}$ was corrected by measuring $^{85}Rb^{+}$ and using $^{87}Rb/^{85}Rb = 0.3861$. During the measurement of Sr isotope compositions of apatite inclusions in zircon, $^{176}Hf^{2+}$ from the host zircon can produce an isobaric interference on $^{88}Sr^{+}$, therefore the constant $^{86}Sr/^{88}Sr$ ratio was monitored throughout the analysis.

Durango apatite, a fluor-apatite (Sr = 450 ppm), was used as the primary reference material. A fluor-apatite MAD (Madagascar apatite) and the in-house characterised hydroxyl-apatite (HA) Holly Springs were used as two secondary reference materials having Sr concentrations of 1650 ppm and 161 ppm, respectively. In the current, study reference materials show no correlation between Sr concentration (Sr intensity) and offset from reported TIMS values, not even in the case of the low-Sr apatite "Holly Springs". Supplementary Fig. 1 demonstrates that the accuracy of the determined Sr isotope ratios are independent of the Sr concentration in the sample and the $^{87}Sr/^{86}Sr$ value of reference materials are within analytical uncertainty of their reported literature values (Fig. 4a & 4b, Supplementary Fig. 1 & 2). Apen et al. (2022) in their LA-MC-ICPMS study of Sr isotopes in apatite found a systematic shift in $^{87}Sr/^{86}Sr$ values of the apatite standards from the values reported from TIMS measurements, after normalization. These offsets can occur due to unresolved interferences of Ca-argides (Horstwood et al., 2008). MAD has a reported $^{87}Sr/^{86}Sr$ value of 0.71180(3) (Yang et al., 2014; 2SD, $n = 11$) and yielded an average value of 0.71177(45) (2SD; $n = 40$) during our measurement session. The reported $^{87}Sr/^{86}Sr$ value of Holly Springs apatite is 0.71893(1) (Emo et al., 2018; 2SD; by TIMS) and during our measurement session $^{87}Sr/^{86}Sr = 0.7189(19)$ (2SD; $n = 30$) was obtained. During analysis Durango apatite was used as a primary reference material to correct for any drift. During the course of the analysis $^{87}Sr/^{86}Sr = 0.706322(642)$ (2SD, $n = 147$) was obtained for Durango apatite, which agrees with the reported $^{87}Sr/^{86}Sr = 0.706328$ (23) (TIMS analyses of Yang et al., 2014; 2SD, $n = 13$), thus no significant bias correction was applied to the data. The agreement of the measured with the recommended value for the primary reference material supports the robustness of the interference correction method followed here. Efficiency of REE^{2+} interference correction was monitored using $^{174}Yb^{2+}/^{86}Sr$ vs $^{87}Sr/^{86}Sr$, which shows no correlation for

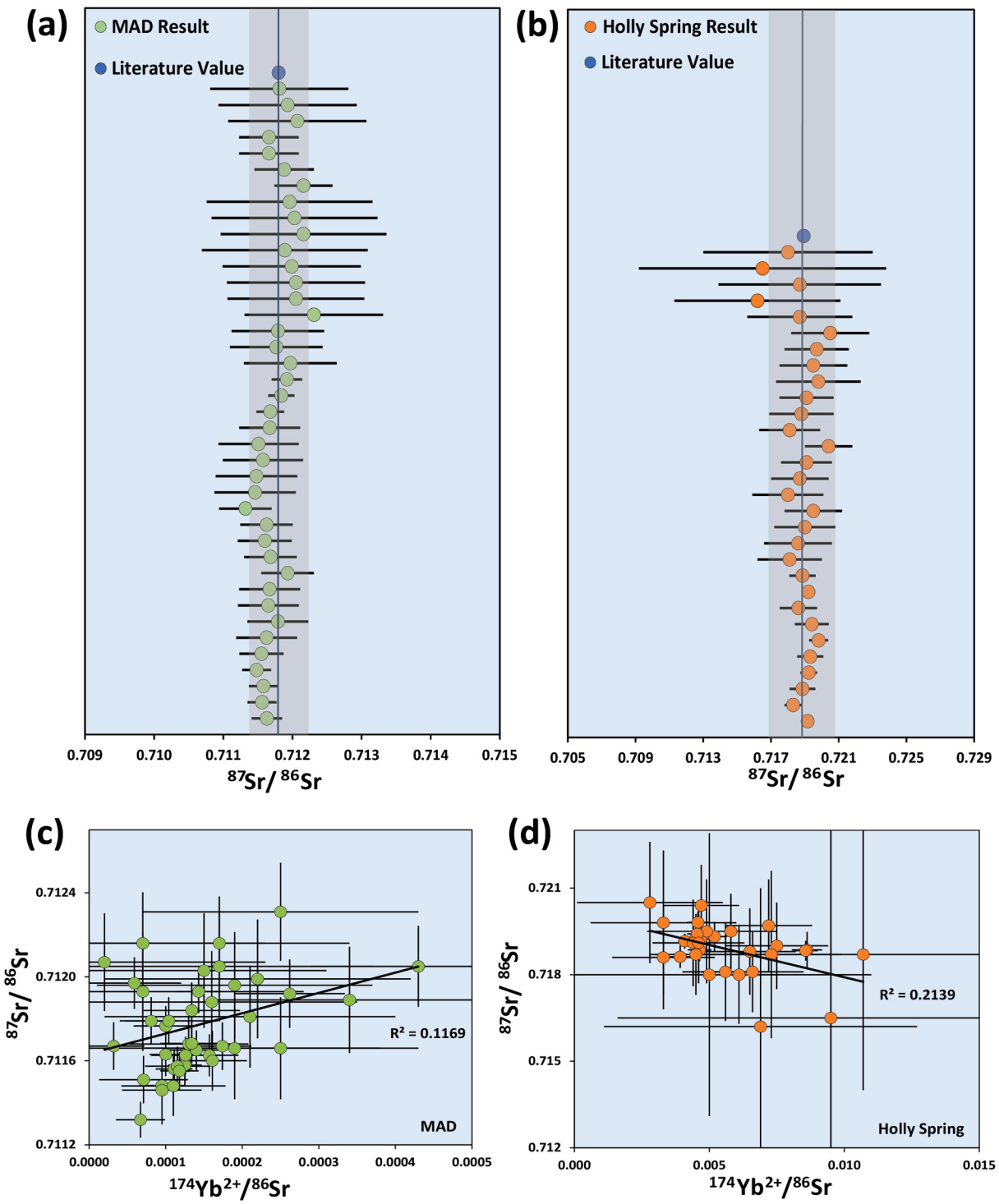

Fig. 4. Standards analysed during this study. (a)- (b) Individual $^{87}Sr/^{86}Sr$ data points of the two secondary standards MAD and Holly Springs measured here with propagated 2SE of individual points. Standards are in good agreement with their literature values (blue marker). (c)-(d) when plotted $^{87}Sr/^{86}Sr$ of individual data points of the two standards do not show any correlation with the REE^{2+} interference monitor $^{174}Yb^{2+}/^{86}Sr$, indicating robustness of the REE interference correction procedure. (For interpretation of the references to colour in this figure legend, the reader is referred to the web version of this article).

both of the secondary apatite standards (Fig. 4c & 4d) and indicates efficient correction for REE^{2+} interferences. In the secondary reference materials, absence of any significant offset of the corrected $^{84}Sr/^{86}Sr$ from the natural $^{84}Sr/^{86}Sr = 0.5650$ indicate the REE^{2+} interference correction protocol was effective. As shown in Supplementary Fig. 2 there is no correlation between the REE^{2+} interference monitor and the shift in $^{87}Sr/^{86}Sr$ ratio of the two secondary reference materials from their representative TIMS values. Furthermore, for the two secondary reference materials, no statistically significant correlation is observed between the uncorrected $^{87}Sr/^{86}Sr$ ratio and individual spot size (Supplementary Fig. 3 a, b).

4. Results

4.1. Mica Rb-Sr ages

The Rb-Sr isotope composition determined from the separated micas from Singhbhum Granites, TTGs, and paragneiss are provided in ST-2. Whole rock Rb-Sr isotope data of these samples are taken from the study of Pandey et al. (2019). Sample OM-27b and Om-29 have whole rock–mica isochron ages of ~3.1–3.2 Ga (Fig. 5 a, b). OM-9b, OM-10b and OM-22 have whole-rock andmica isochron ages ~2.4 Ga (Fig. 5 c, d, e).

4.2. Petrography of matrix apatite and apatite inclusions

Single matrix apatite grains were studied with both SEM and transmitted light microscope. Most of the apatite grains are euhedral to subhedral (Fig. 2) with sizes ranging from 50 to 300 μm. In some of the samples, apatite grains have multiple inclusions of other minerals such as zircon (Fig. 2a, c), biotite (Fig. 2e), albite, monazite, or quartz; and some have multiple fluid inclusion trails (Fig. 2d). In most cases, the inclusions are beneath the exposed surface and can neither be detected by CL nor by BSE imaging (Fig. 2a), thus transmitted light images of individual grains are needed. By combining BSE and transmitted-light images, laser spot placement can be optimised in order to obtain the best-preserved initial $^{87}Sr/^{86}Sr$ value (Fig. 2b). Fig. 2c shows the direct effect of disturbance caused by a laser spot in an apatite placed on an inclusion of mica and zircon, as the spot OM21–17 gives $^{87}Sr/^{86}Sr$ = 0.70668(89), which is the highest measured value for that sample. In contrast spot OM21–18 in the same sample has $^{87}Sr/^{86}Sr$ = 0.70069(58) (a shift of 8.5‰), which appears to be the best-preserved value for initial $^{87}Sr/^{86}Sr$. In addition, as shown in Fig. 2d and Fig. 2e, fluid inclusion trails and cracks in apatite grains filled with mica, when ablated, yield an $^{87}Sr/^{86}Sr$ value elevated by tens of per mil.

Apatite inclusions were selected only from those zircon crystals that

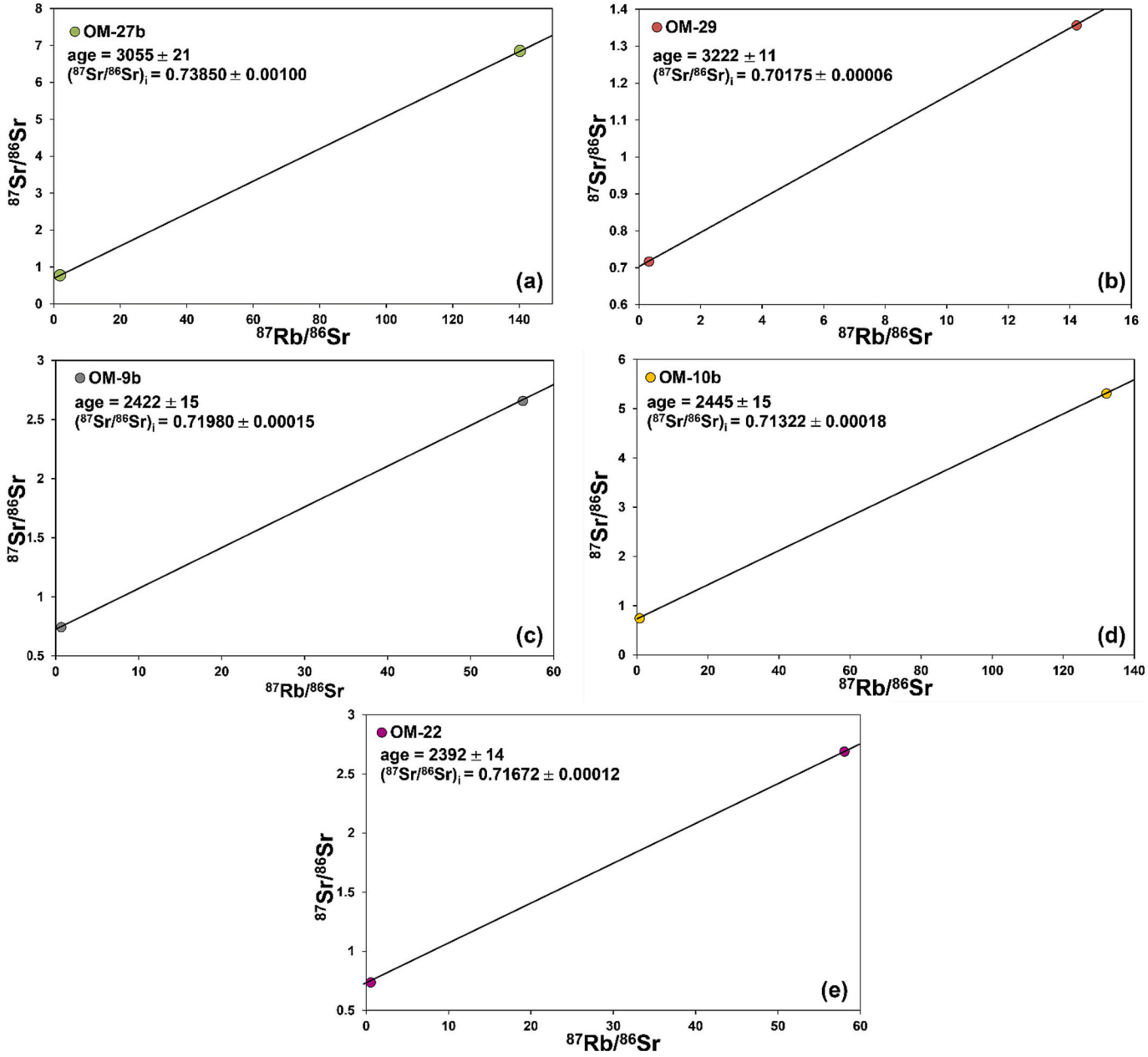

Fig. 5. Rb-Sr isochron diagrams. All isochron ages are in Ma. (a) & (b) Whole-rock (Pandey et al., 2019) and mica (this study) isochron of samples OM-27b and OM-29. These samples preserve Rb-Sr mica cooling age. (c, d, e) Whole-rock and mica isochron for samples OM-9b, OM-10b and OM-22.

preserved primary igneous zoning (Fig. 3 c-f). In addition, only those apatite inclusions that were fully encapsulated within zircon were analysed. This was done to maximize the potential to determine the initial Sr isotope compositions. For grains like those shown in Fig. 3a & 3b, where healed fractures within the zircon grain are in contact with the apatite inclusion, there is an increased chance that the Sr isotope composition is reset.

4.3. Apatite $^{87}Sr/^{86}Sr$ analyses

All Sr isotope data obtained for matrix apatite and apatite inclusions in zircon are shown in Table ST-5. For all samples, the measured $^{87}Sr/^{86}Sr$ show some variation within a sample, indicating that there is some disturbance of the $^{87}Sr/^{86}Sr$ and thus the measured isotope ratio cannot correspond to $^{87}Sr/^{86}Sr_i$ in all cases. This spread can be due to a true variation of the $^{87}Sr/^{86}Sr$ in a given crystal caused by (partial) re-equilibration resulting from later thermal overprint.

Apatite inclusions have commonly higher $^{87}Rb/^{86}Sr$ ratios compared to matrix apatite grains (Fig. 6a). Elevated Rb in apatite can be caused by ablating hidden inclusions that are high in Rb or by low-grade over-printing through fluid interactions with the apatite inclusion itself. However, there is no correlation between $^{87}Sr/^{86}Sr$ and $^{87}Rb/^{86}Sr$ (Fig. 6a) in the measured samples, which shows successful correction of the Rb interference. Analyses that have elevated Rb typically also have larger uncertainties, which is a combined effect of the additional corrections that need to be applied to those data and the fact that smaller spot sizes were chosen for the apatite inclusions. Analyses with elevated Rb content are excluded from further data treatment as the primary nature of the apatite grains cannot be guaranteed for these measurements.

Ablating the host zircon along with an apatite inclusion results in an increased REE^{2+} interference of $^{174}Yb^{2+}$ on ^{87}Sr. Fig. 6b shows that analyses with high $^{174}Yb^{2+}/^{86}Sr$ commonly also have elevated $^{84}Sr/^{86}Sr$ values which can be due to incomplete corrections for doubly charged REE^{2+} interferences. Due to the low abundance of ^{84}Sr, this ratio is more sensitive to REE^{2+} interferences. Fig. 6b further shows that samples with measured $^{84}Sr/^{86}Sr$ close to the natural value of 0.0565, also have very low $^{174}Yb^{2+}/^{86}Sr$ (black area marked in Fig. 6b). These are the samples, that can reliably be corrected for REE^{2+} interference and are considered for further data processing and discussion.

Fig. 6c and d can be used to visualise the filtering approach followed here. Rough trends towards the y-axis (sector-1) indicate ablation of hidden inclusions along with apatite, and trends towards the x-axis (sector-3) indicate a high amount of host zircon ablation during apatite inclusion measurement resulting in high REE^{2+} interference, whereas data plotting between the two trends indicate mixed influences (sector-

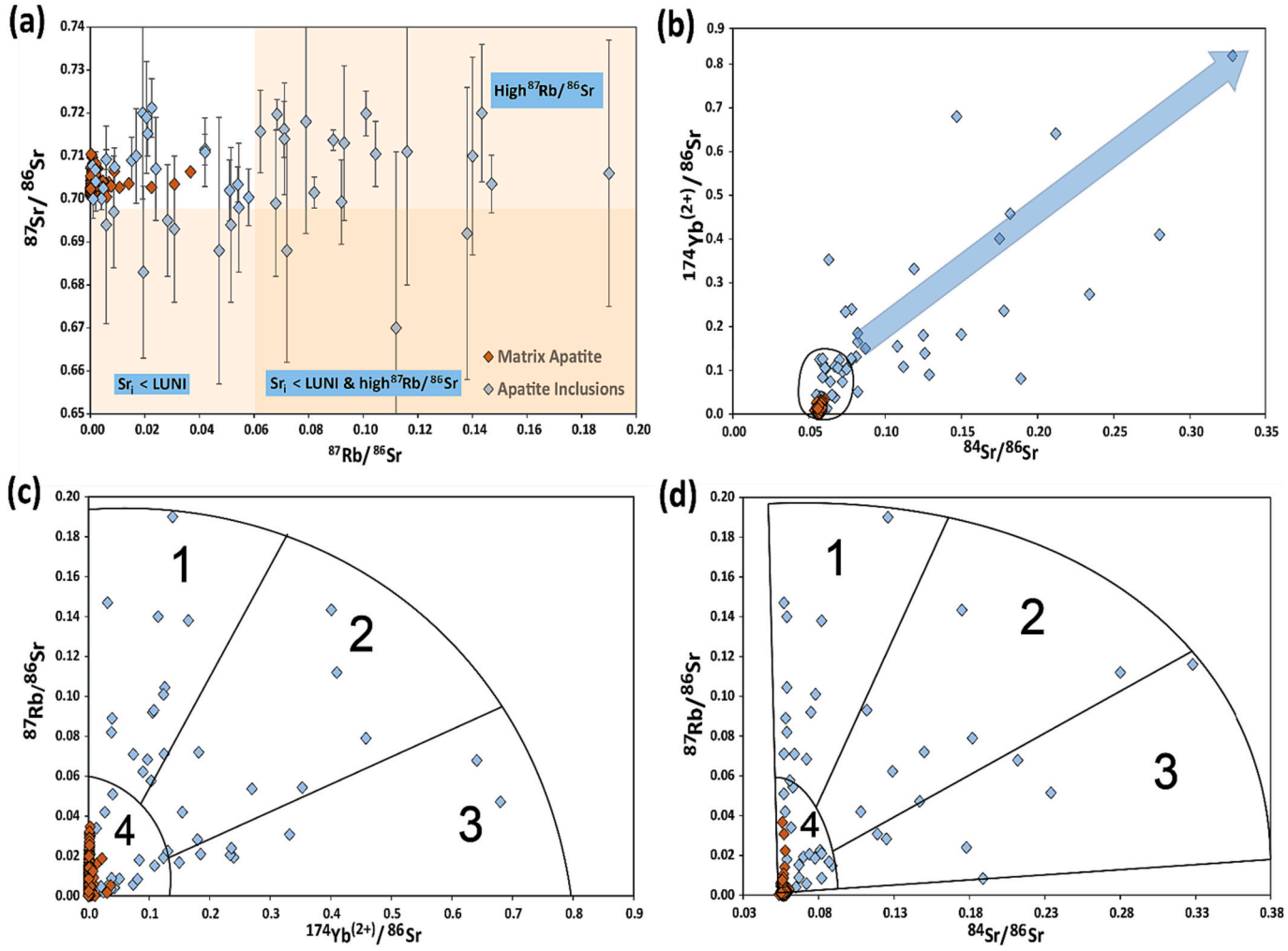

Fig. 6. Apatite LA-MC-ICPMS data processing. (a) Apatite inclusions in zircon showing larger scatter in $^{87}Rb/^{86}Sr$ in $^{87}Sr/^{86}Sr$ vs $^{87}Rb/^{86}Sr$ space. Sectors indicated in orange are values with either very high $^{87}Rb/^{86}Sr$, not reasonable for apatite, or $^{87}Sr/^{86}Sr$ values lower than the Lunar initial (LUNI), or both. (b) $^{174}Yb^{2+}/^{86}Sr$ vs $^{84}Sr/^{86}Sr$ show co-variation. Samples having $^{84}Sr/^{86}Sr$ close to natural value show very restricted variation in $^{174}Yb^{2+}/^{86}Sr$, whereas higher $^{84}Sr/^{86}Sr$ correlate with large scatter in $^{174}Yb^{2+}/^{86}Sr$, indicating higher REE^{2+} isobaric interference. (c)- (d) are used to filter out samples with higher $^{174}Yb^{2+}/^{86}Sr$ indicating high REE^{2+}interference and samples with high $^{87}Rb/^{86}Sr$ indicative of ablating other mineral phases along with apatite.

2). Analyses plotting in sector-4 in Fig. 6c and Fig. 6d are samples with low $^{87}Rb/^{86}Sr$ along with low $^{174}Yb^{2+}/^{86}Sr$ and $^{84}Sr/^{86}Sr$ close to the natural value. Samples meeting these criteria (sector-4) are further processed to derive the "best-preserved initial $^{87}Sr/^{86}Sr$".

After filtering the measured $^{87}Sr/^{86}Sr$ values by applying these criteria (Supplementary Fig. 4a) they were age-corrected, based on the measured $^{87}Rb/^{86}Sr$. For both matrix apatite and apatite inclusions in zircon, the age correction mostly resulted in $\Delta^{87}Sr/^{86}Sr < 0.6‰$, with only 11 out of 270 apatite spot analyses showing a change in $^{87}Sr/^{86}Sr$ of >0.6‰. Samples for which the U-Pb ages are taken from Pandey et al. (2019), the same hand specimens in which zircon U-Pb data had been obtained before, were used to extract matrix apatite and zircon with apatite inclusions. Samples, for which the assigned ages are from Upadhyay et al. (2014), were collected either from the same outcrop or from the same geologic unit (see Pandey et al., 2019). The age of 3.262 (4) Ga, assigned to the Badampahar Group basaltic andesite sample OM-4a, is the maximum depositional age of a conglomerate that stratigraphically underlies the basaltic andesite. The depositional age was calculated (Supplementary Fig. 5) using detrital zircon U-Pb age data of the conglomerates from Frimmel et al. (2022).

Following the age correction, some of the lowest $^{87}Sr/^{86}Sr$ values overlapping within analytical uncertainties were grouped (average; ST-6) to obtain representative $^{87}Sr/^{86}Sr_i$ for a particular sample (Supplementary Fig. 4b; ST-6). Taking the average of the lowest $^{87}Sr/^{86}Sr$ values to represent the $^{87}Sr/^{86}Sr_i$ of a sample ensures high $^{87}Sr/^{86}Sr$ values resulting from later alteration events are selectively left out (Giuliani et al., 2020; Ravindran et al., 2020). These $^{87}Sr/^{86}Sr_i$ are maximum estimated values for the true $^{87}Sr/^{86}Sr_i$. Within all the samples analysed, nine have low $^{87}Sr/^{86}Sr_i$ preserved in matrix apatite grains, and in four samples preserved $^{87}Sr/^{86}Sr_i$ has been measured from apatite inclusions in zircon (ST-5&6). OM-8 and OM-10a, the two oldest rock samples analysed in this study, have an age of 3.44 Ga and $^{87}Sr/^{86}Sr_i$ of 0.6999 (26) (2SE) and 0.70043(95) (2SE), respectively. The combined matrix apatite and apatite inclusions data from them yielded $^{87}Sr/^{86}Sr_i$ = 0.70029(63) (2SE) (Table 1). Younger samples show progressively more radiogenic $^{87}Sr/^{86}Sr_i$ isotope compositions (Table 1, Fig. 7). The youngest granitoid sample OM-18 with an age of 3.292(19) Ga yielded $^{87}Sr/^{86}Sr_i$ = 0.70163(38) (2SE). The sample from Badampahar group analysed in this study is the 3.262(4) Ga (Supplementary Fig. 5) old basaltic andesite OM-4a, from which matrix apatite was measured and gave a very precise initial $^{87}Sr/^{86}Sr$ value of 0.70078(6) (2SE).

5. Discussion

The emplacement ages of the different felsic crustal units of the Singhbhum Craton are well constrained (e.g., Upadhyay et al., 2014; Dey et al., 2017; Chaudhuri, 2020; Hofmann et al., 2022; Mitra et al., 2022), but the composition and timeline of formation and differentiation of their precursor(s) and the age and composition of the source(s) of precursor(s) are under discussion. Pandey et al. (2019) concluded that the mafic precursor of the Singhbhum TTGs and granites was sourced from a near-chondritic mantle at ~3.5 Ga. Partial melting of this mafic precursor subsequently led to the formation and emplacement of the TTG suite. Dey et al. (2017) suggested extraction of the mafic precursor for the older TTGs from a depleted mantle with $^{176}Lu/^{177}Hf = 0.0113$ at ~3.6 Ga. After emplacement, this TTG suite was reworked to form the Singhbhum Suite of granites. Upadhyay et al. (2019) concluded that the TTGs and Singhbhum Granites were derived from two different sources, a juvenile mafic crust and pre-existing Eoarchean TTG crust, respectively. The Hadean and Eoarchean xenocrystic zircons in tonalite gneisses of the Champua Suite yielded εHf_i of −6.6 to −1.5 (Chaudhuri et al., 2018), indicating the presence of Hadean enriched proto-crust in the source of these TTGs. Maltese et al. (2022) in their study based on coupled $^{147,146}Sm$–$^{143,142}Nd$ using the same samples studied here, showed that Singhbhum TTGs and supracrustal rocks were derived from a depleted mantle source, which had undergone mantle differentiation in the Hadean at ~4.2 Ga. The present study hence focuses on better understanding the evolution of different precursor materials, which ultimately led to the formation of Paleoarchean felsic crustal nucleus of Singhbhum Craton.

5.1. Assessing primary $^{87}Sr/^{86}Sr$ in apatite

The Rb-Sr system is sensitive to overprinting by later tectonothermal events. Therefore, an assessment is needed to evaluate the extent of preservation of $^{87}Sr/^{86}Sr_i$ in matrix apatite grains and apatite inclusions in zircon, before using them to extract geologically significant information. Since Sr in apatite can re-equilibrate in the matrix even during low-grade thermal overprint or via re-crystallization, it is essential to establish the time of the last significant thermal overprint. The closure temperature for Sr diffusion in apatite is expected to be similar or higher than in mica. Thus, mica ages from the same sample provide robust information on the closure of the Sr isotope systematics in apatite (Cherniak and Ryerson, 1993; Cherniak, 2000).

Studies on the Singhbhum Craton have hinted towards last significant thermal overprint in cratonic scale in the Mesoarchean (Prabhakar and Bhattacharya, 2013; Upadhyay et al., 2014; Pandey et al., 2019; Bose et al., 2021). Later low grade thermal overprint is mostly local (Upadhyay et al., 2014). This contrasts with other Paleo- to Mesoarchean crustal segments in different cratons worldwide that were overprinted by high-grade metamorphic events in the Neoarchean or even the Proterozoic (Sano et al., 1999), making it difficult to derive initial isotope compositions for rocks and minerals corresponding to the time of emplacement.

One of the first ages for the Singhbhum Craton is from Moorbath et al. (1986), who determined a Rb-Sr mica age of 3.28(13) Ga from the TTGs of the Champua area. Later, Vohra et al. (1991) showed that the Kaptipada granite has a Rb-Sr mica age of 3.275(81) Ga and Upadhyay et al. (2014) determined a U-Pb age of 3.317(8) Ga for metamorphic rutile from the high grade Badampahar group. Pandey et al. (2019) determined the common Pb isotope compositions of feldspar grains in the same samples used in this study, and showed a very narrow range in $^{206}Pb/^{204}Pb$, $^{207}Pb/^{204}Pb$ and $^{208}Pb/^{204}Pb$ ratios. This indicates that Paleoarchean Singhbhum granitoids have efficiently preserved close to initial Pb isotope ratios on the whole craton scale from ~3.2 Ga till present. U-Pb monazite ages (Prabhakar and Bhattacharya, 2013) from the high grade Badampahar rocks (OMGs) also indicate that the last major high grade overprinting in the Singhbhum Craton likely happened at 3.2–3.3 Ga.

In order to evaluate the thermal history of the whole Singhbhum Craton, biotite and muscovite from (meta)igneous rocks were separated for Rb-Sr dating. The Rb-Sr whole rock mica isochron ages of samples from Singhbhum granitoids and meta sediments define two age groups (Fig. 5), one at 3.1–3.2 Ga (Fig. 5 a, b) and the other at ~2.4 Ga (Fig. 5 c, d, f). Since, U-Pb zircon ages of these samples are 3.292(19) Ga or older (Pandey et al., 2019), whole rock-mica isochron ages represent cooling ages, defining the time when the samples cooled below ~400–350 °C (e.g. Nebel et al., 2011). Rutile has a closure temperature for Pb between ~400 °C (Mezger et al., 1989) and ~ 600 °C (Kooijman et al., 2010). Therefore, the Rb-Sr ages together with the monazite Th-U-Pb ages (Prabhakar and Bhattacharya, 2013), U-Pb rutile ages (Upadhyay et al., 2014) and feldspar Pb isotope composition (Pandey et al., 2019) of Singhbhum granitoids and meta-sediments indicate that the terrane was not affected significantly by any high grade thermal overprinting after 3.1 Ga in the west. Whereas the eastern part of the craton has been affected by a more recent 2.4 Ga metamorphic event. Other studies based on tectonic evolution of the Singhbhum craton and surrounding mobile belts have also indicated the lack on any high-grade metamorphic over printing in the cratonic nucleus after 3.1–3.2 Ga (Bose et al., 2021; Ghosh and Bose, 2020).

The distribution of the Rb-Sr mica ages combined with very low $^{87}Sr/^{86}Sr_i$ indicates that the Singhbhum Suite in the western part of the

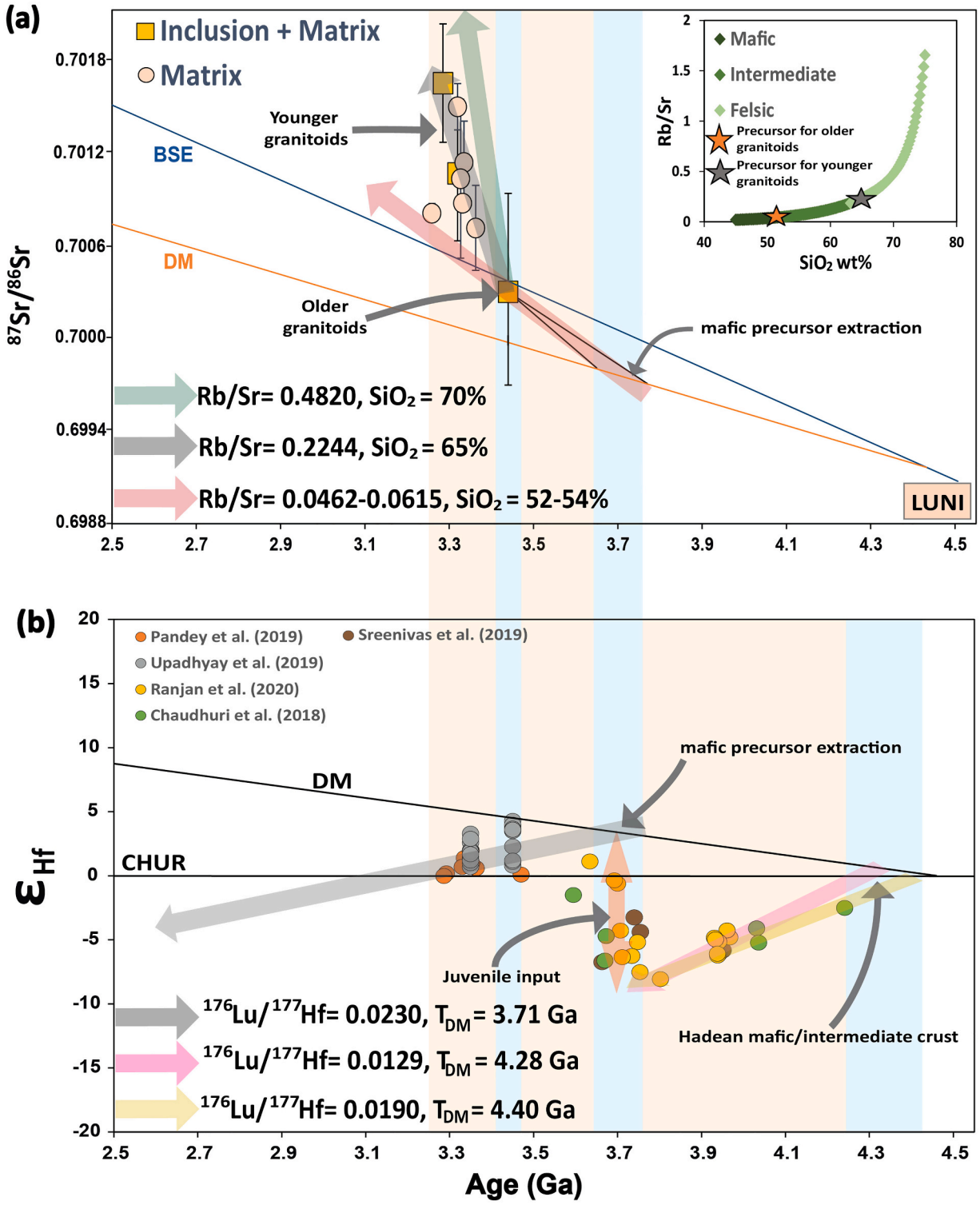

Fig. 7. (a) Measured initial $^{87}Sr/^{86}Sr$ of Paleoarchean felsic rocks from the Singhbhum Craton. Three different arrows indicate Sr isotope evolution of three different precursors with varied SiO_2 content and initial Rb/Sr. Figure in the inset depicts the correlation of SiO_2 content of a rock with its Rb/Sr. Lunar Initial $^{87}Sr/^{86}Sr_{LUNI}$ = 0.699072 (Carlson and Lugmair, 1988) represents the $^{87}Sr/^{86}Sr_i$ of BSE (Mezger et al., 2021). Present day $^{87}Sr/^{86}Sr_{BSE}$ = 0.7045 and $^{87}Sr/^{86}Sr_{DMM}$ = 0.70263 (McDonough and Sun, 1995; Workman and Hart, 2005). Half-life of $^{87}Rb = 1.393 \times 10^{-11}$ a^{-1} (Nebel et al., 2011) (b) Compiled Singhbhum whole rock and in-situ zircon Hf initial data in εHf space. Three Hf evolution curves (grey, pink and yellow) indicate extraction age, initial $^{176}Lu/^{177}Hf$ and time dependent evolution of different precursors. Vertical arrow indicates juvenile mafic crust extraction from the depleted mantle at ~3.7 Ga, which matches the precursor extraction age for the Paleoarchean felsic crustal nuclei of Singhbhum. Alternating orange and blue vertical blocks matching both in initial Sr and initial Hf isotope space, indicate alternating source extraction and precursor evolution. Present day $(^{176}Hf/^{177}Hf)_{DM}$ = 0.28325 (Griffin et al., 2000), and present day CHUR parameter $(^{176}Hf/^{177}Hf)_{CHUR}$ = 0.282785 and $(^{176}Lu/^{177}Hf)_{CHUR}$ = 0.0336 (Bouvier et al., 2008). Half-life of $^{176}Lu = 1.86 \times 10^{-11}$ a^{-1} (Scherer et al., 2001). (For interpretation of the references to colour in this figure legend, the reader is referred to the web version of this article).

craton has a better preservation potential for $^{87}Sr/^{86}Sr_i$ in matrix apatite than in the eastern and southern part of the craton (Fig. 1). Sample OM-29, which has a U-Pb zircon age of 3.363(12) Ga (Pandey et al., 2019), yielded an approximately 100 Ma younger whole rock-mica isochron age (Fig. 5b). The measured $^{87}Sr/^{86}Sr_i$ of matrix apatite in this sample is 0.7007(3), whereas the whole rock-mica isochron initial for this sample is 0.70175(6). Sample OM-22 represents an intrusive phase of the Singhbhum Suite (Singhbhum Granite Phase-II) and has a Rb-Sr mica isochron age of 2.392(14) Ga (Fig. 5e). The matrix apatite crystals from this sample preserve low $^{87}Sr/^{86}Sr_i = 0.70102(51)$, which is much lower than the whole rock-mica isochron initial of 0.71672(12). This indicates preservation potential of primary $^{87}Sr/^{86}Sr_i$ in apatite even when whole rock and mica $^{87}Sr/^{86}Sr_i$ have later been overprinted. In the samples OM-10a, OM-18 and OM-21, apatite inclusions and matrix apatite crystals were measured (ST-6). The $^{87}Sr/^{86}Sr_i$ values in these individual samples do not show any significant variation between matrix apatite and apatite inclusions in zircon (only 0.9‰ to 2‰), whereas, apatite crystals with overprinted isotope signatures in TTGs from Acasta Gneiss Complex (Emo et al., 2018) show around 20‰ difference in $^{87}Sr/^{86}Sr_i$ between matrix apatite and apatite inclusions in zircon. The mica and apatite Sr isotope data are compared in the Singhbhum samples and only those with preserved $^{87}Sr/^{86}Sr_i$ (samples marked in blue in Fig. 1) are used for further discussion. Almost all samples that preserve the most primitive $^{87}Sr/^{86}Sr_i$ in the Singhbhum Craton are from the western part of the craton (Fig. 1). This observation also matches with the mica Rb-Sr data, indicating that the western part of the Singhbhum Craton is more pristine than the eastern part.

5.2. Precursor for Singhbhum TTGs and granites

Voluminous Paleoarchean granitoids constitute the nucleus of the present-day Singhbhum Craton and belong to two distinct generations. The older 3.53–3.44 Ga granitoids are mostly Na-rich TTGs with a minor low-potassic ($K_2O/Na_2O < 0.81$) granitic component, whereas the younger 3.4–3.2 Ga granitoids are mostly K-rich (K_2O/Na_2O = 1.03–1.57) granites (Singhbhum Granite phases/ Singhbhum Suite) with a minor TTG component (Upadhyay et al., 2019). The older granitoids in the field show evidence of partial melting, melt migration and contain mafic inclusions (Supplementary Fig. 6). To ensure Hf_i is taken from material that is co-magmatic with apatite in which $^{87}Sr/^{86}Sr_i$ is measured, the Hf_i from zircon obtained by Pandey et al. (2019) is taken, whereas Hf_i from Upadhyay et al. (2019) is taken to represent the only whole rock Hf isotope data of the Singhbhum granitoids (Fig. 7b). The combined Hf isotope data show progressive and systematic decrease in εHf_i towards younger granitoids (Fig. 7b). This change of Hf_i in these Paleoarchean granitoids is consistent with a precursor extracted from a depleted mantle source at ~3.71 Ga with $^{176}Lu/^{177}Hf = 0.023$ (see Supplementary Text- Section. 4 for the modelling approach), which is similar to the representative $^{176}Lu/^{177}Hf = 0.022–0.021$ for average Archean mafic crust (Amelin et al., 1999; Gillespie et al., 2021a). Instead of a single age, a range of 3.77–3.65 Ga is considered for the extraction of the precursor for the granitoids. This requires a range in initial $^{176}Lu/^{177}Hf = 0.020–0.025$ to agree with the Hf_i obtained for the granitoids (grey evolution curve in Fig. 7b). $^{87}Sr/^{86}Sr_i$ measured on the same granitoids also show progressively more radiogenic values with younger age (Fig. 7a). The older granitoids in the Singhbhum Craton yielded $^{87}Sr/^{86}Sr_i = 0.70029(63)$ (Table 1). Taking 3.77–3.65 Ga from Hf isotope modelling (Supplementary Text- Section. 4) as the range of the possible precursor extraction age for the granitoids, Sr isotope modelling shows the range in $^{87}Rb/^{86}Sr$ needed for that precursor rock to evolve to $^{87}Sr/^{86}Sr = 0.70029$ by 3.44 Ga after extraction from the mantle is 0.134–0.178 (pink evolution line Fig. 7a). This equates to a range in Rb/Sr from 0.0462 to 0.0615, implying a precursor SiO_2 content of ~52–54 wt% (Fig. 7a). As shown in the inset of Fig. 7a, this range in SiO_2 content is indicative of a rock plotting in the upper mafic to lower intermediate field in the global compilation of Rb/Sr vs SiO_2 content of rocks (Dhuime et al., 2015). Published data from the Paleoarchean rocks of varied compositions from the Singhbhum Craton puts the precursor for the older granitoids in the mafic field (Fig. 8). Having a mafic rock as the precursor for older granitoids also justifies the assumed range of $^{176}Lu/^{177}Hf = 0.020–0.025$ for that precursor, which is the range in $^{176}Lu/^{177}Hf$ for mafic crust. This result agrees with other studies, which indicate Archean TTGs formed mostly by reprocessing of older mafic crust (O'Neil and Carlson, 2017; Vezinet et al., 2018). Once the uncertainty (external 2SE) in the measured $^{87}Sr/^{86}Sr_i$ of the older granitoids is taken into account, the lowest values can be modelled (Supplementary Text- Section. 4) with a precursor having Rb/Sr = 0.105, which formed around 4.2 Ga. Presence of Hadean crust has

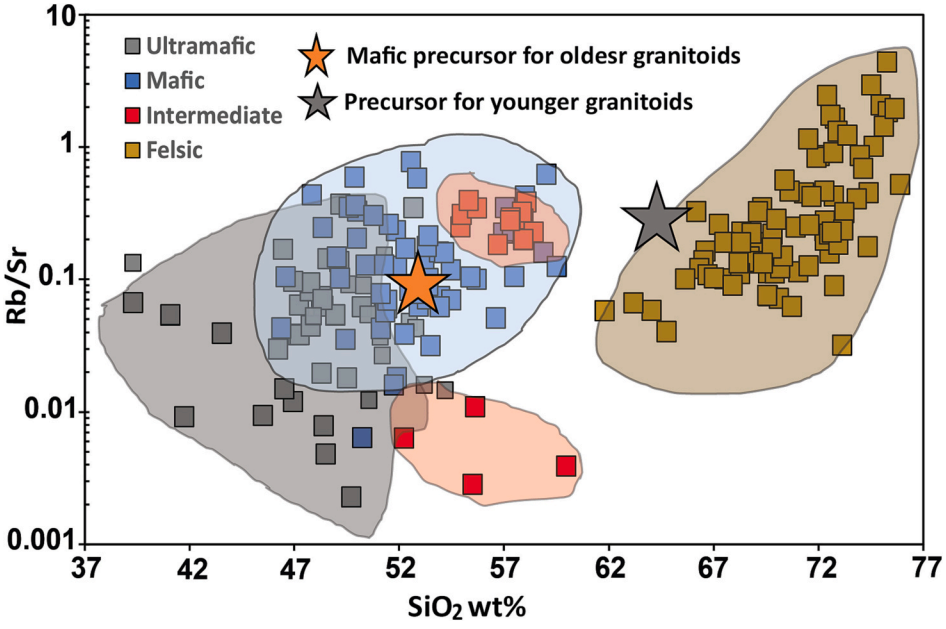

Fig. 8. Rb/Sr vs SiO_2 wt% plot for compiled data from Paleoarchean rocks in the Singhbhum Craton. Colours of the two stars indicate the composition of two precursors used for the evolution curves in Fig. 7a.

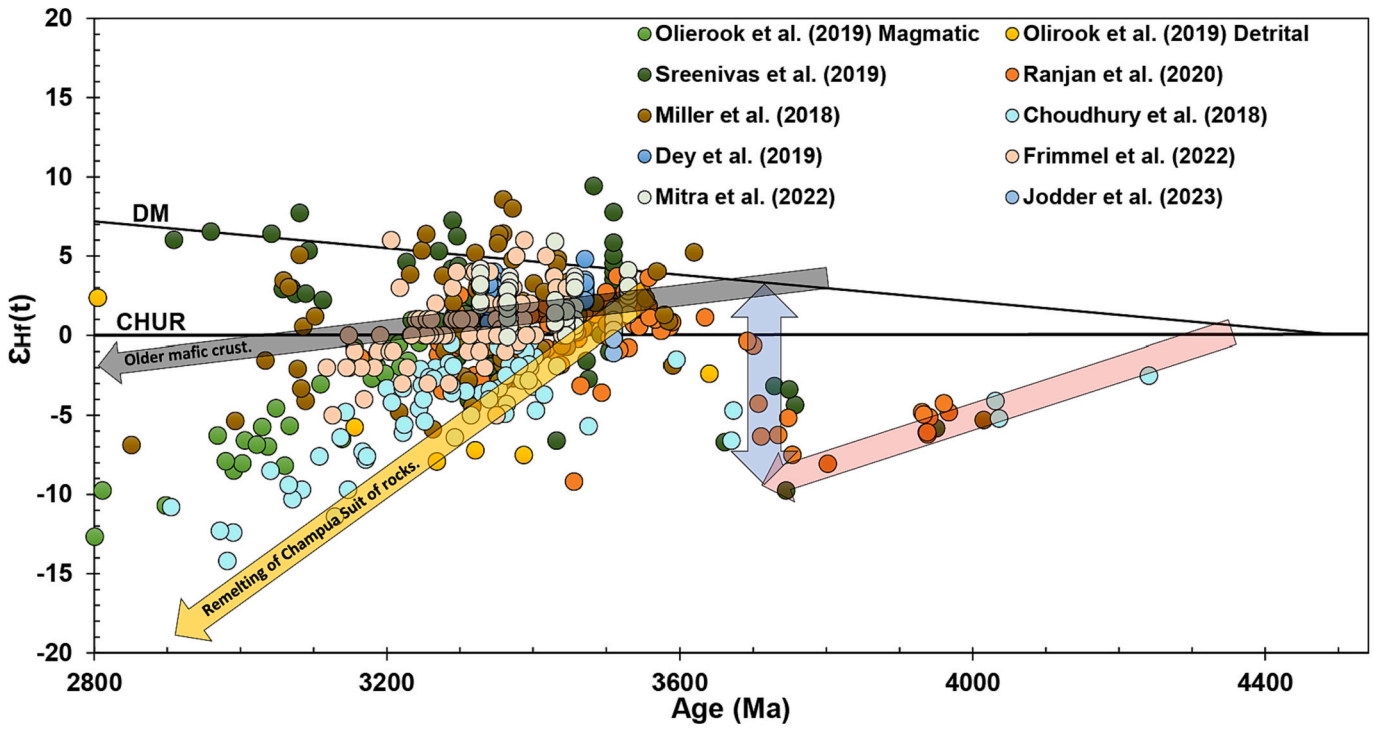

Fig. 9. Compilation of detrital and igneous zircon εHf_i data from Singhbhum Craton. The grey evolution line indicates the modelled mafic source extraction and evolution. The yellow line represents the evolution line for the older TTGs that were produced between 3.53 and 3.44 Ga. (For interpretation of the references to colour in this figure legend, the reader is referred to the web version of this article)

already been suggested for the Singhbhum Craton by multiple previous studies (Chaudhuri et al., 2018; Miller et al., 2018; Sreenivas et al., 2019; Ranjan et al., 2020b; Maltese et al., 2022). The highest $^{87}Sr/^{86}Sr$ can be modelled with a precursor formed between 3.77 and 3.65 Ga with Rb/Sr between 0.0934 and 0.136, which equates to a rock having a SiO_2 content between ~57 and ~62 wt%. This observation is in line with previous studies (Upadhyay et al., 2014; Chaudhuri et al., 2018; Upadhyay et al., 2019) that indicate the presence of older evolved material as one of the precursors of the 3.44 Ga old TTGs. The contribution of this older evolved material was likely volumetrically minor. This is because significant contributions from the older evolved material would have shifted the $^{87}Sr/^{86}Sr_i$ of the oldest TTGs to much higher values than measured here. Hence, even if multiple precursors were involved in generating the older granitoids, those mostly had similar SiO_2 contents (more mafic than felsic) and lower Rb/Sr so that the mixed sources would evolve to the measured $^{87}Sr/^{86}Sr_i$ at 3.44 Ga for the TTGs. Fig. 9 shows the modelled mafic precursor extraction between 3.77 and 3.65 Ga. Evolution of this modelled mafic precursor is also consistent with the compiled Hf_i data in zircon from the Singhbhum Craton.

The $^{87}Sr/^{86}Sr_i$ in granitoids is a very sensitive parameter that traces the compositional evolution of their precursors, particularly when slightly enriched precursor materials have only short crustal residence times. This results in only minor changes in $^{176}Hf/^{177}Hf$ and $^{143}Nd/^{144}Nd$, the most commonly used isotope systems to study Archean rocks. The sensitivity of the $^{87}Sr/^{86}Sr$ is due to much stronger fractionation of Rb/Sr during partial melting and subsequent differentiation, whereas the elemental pairs Lu-Hf and Sm-Nd show large fractionation during mantle melting but only minor fractionation during subsequent magmatic differentiation or reprocessing of enriched crustal material. This can be illustrated with the combined Sr_i – Hf_i evolution of the younger granitoids. Fig. 7 shows that the $^{176}Hf/^{177}Hf$ evolution for all granitoids can be modelled using one single precursor evolution. However, modelling the same mafic precursor evolution with Sr isotopes (pink evolution line Fig. 7a) show that younger granitoids are too radiogenic to be produced by reprocessing of only the older mafic precursor. Hence, though undetected in the Hf isotope space (for the samples studied here), the Sr isotope evolution of these granitoids record a shift in the precursor composition between emplacement of older and younger granitoids. The older granitoids have SiO_2 contents of ~70 wt% (Pandey et al., 2019), indicating their evolution to very radiogenic $^{87}Sr/^{86}Sr_i$ of ~0.70314 by 3.292 Ga (green evolution curve Fig. 7a). Thus, the younger granitoids are also not the product of reprocessing of only the older granitoids. However, the Sr isotope evolution of the granitoids from $^{87}Sr/^{86}Sr_i = 0.70029$ at 3.44 Ga to $^{87}Sr/^{86}Sr_i = 0.70163$ at 3.292 Ga can be modelled (grey evolution curve Fig. 7a) using a precursor with Rb/Sr = 0.2244 at 3.44 Ga. This equates to a precursor for the younger granitoids with ~64–65 wt% SiO_2, indicative of an intermediate to felsic (inset Fig. 7a) composition. In the compiled Singhbhum rock dataset (Fig. 8), this precursor composition of the younger granitoids plot between the mafic and felsic fields (towards the boundary of the felsic field). Hence, in both the Sr isotope evolution model (Fig. 7a) and in Rb/Sr vs SiO_2 space, the modelled composition of the precursor for younger granitoids plot between a mafic precursor and older granitoids. This observation, combined with the field evidence of partial melting of older granitoids (Supplementary Fig. 6), melt migration, presence of mafic enclaves within the partial melt generated from granitoids (magma mingling) (Supplementary Fig. 6), indicate that the younger granitoids were generated by mixing of melts derived from the older mafic precursor with melts generated by intra-crustal reworking of the older granitoids. Emplacement of the younger granitoids (Suighbhum Suite granite) is also contemporaneous with the amphibolite facies metamorphism of older granitoids in the Champua area (Prabhakar and Bhattacharya, 2013; Upadhyay et al., 2014). This tectono-metamorphic relation between the two lithounits further support the notion that older granitoids acted as one of the precursors for the younger granitoids. Upadhyay et al. (2019) also pointed towards a mixed (mafic and felsic) crustal source for the younger granitoids formed between 3.4 and 3.2 Ga. Samples studied by Chaudhuri et al. (2018) have consistently more negative εHf_i values (Fig. 9), indicating those samples represent the younger granitoids generated only by intra-crustal reworking of the

older granitoids (yellow evolution line Fig. 9), which is in line with field evidence (Supplementary Fig. 6a).

A basaltic andesite from the Gorumahisani greenstone belt with an age of 3.262 (4) Ga (OM-4a) gave a very precise and unradiogenic initial $^{87}Sr/^{86}Sr = 0.70078(6)$ (2SE; Fig. 7a). This indicate that the mafic and ultramafic rocks in this greenstone belts most likely had a source distinct from that of the granitoids surrounding the greenstone belt lithologies, although having formed in a similar temporal framework.

5.3. Perspective on craton evolution

Rare Eoarchean detrital zircon crystals and Eoarchean to Hadean zircon xenocrysts in magmatic rocks have been found in different sedimentary units and in the Champua Suite (Chaudhuri et al., 2018; Sreenivas et al., 2019; Ranjan et al., 2020b). The Hf isotope composition of these zircon grains/crystals provide information on the Eoarchean and Hadean crustal evolution of the Singhbhum Craton prior to the major interval of felsic crust formation and reworking between 3.53 and 3.2 Ga. Rocks with such old zircon crystals have not been found in the craton. Evidence for the existence of Eoarchean to Hadean rocks is only preserved in these rare single zircon grains and the location of their source rock(s) is unknown. The Hf_i measured in these detrital and magmatic zircons record an Eoarchean to Hadean enrichment process (Chaudhuri et al., 2018; Sreenivas et al., 2019; Ranjan et al., 2020b). These Hf_i define a trend, that can be modelled (Fig. 7b) with a precursor extraction at ~4.28 Ga from the fertile mantle (BSE/CHUR) with an initial $^{176}Lu/^{177}Hf = 0.0129$ or at 4.4 Ga with initial $^{176}Lu/^{177}Hf = 0.0190$ (Chaudhuri et al., 2018). This modelled range in $^{176}Lu/^{177}Hf$ value for the Hadean precursor material indicates formation of mafic and evolved (intermediate) crustal material in the Hadean (Fig. 10a, adapted from Bauer et al., 2020). This conclusion is also supported by $^{147,146}Sm$–$^{143,142}Nd$ systematics reported by Maltese et al. (2022), on the same granitoid samples studied here. They found evidence for a 4.2 Ga crust-mantle differentiation event in the Singhbhum Craton, which led to formation of a depleted mantle that later acted as a source for the Paleoarchean granitoids. Hafnium isotope data from these Hadean to Eoarchean zircons combined with short- and long-lived Sm-Nd isotope studies of Paleoarchean granitoids, support the presence of an evolved crustal unit already in the early Eoarchean, as the first crustal nucleus of the craton (Fig. 10a). The fact that this early enrichment is not recorded in the $^{87}Sr/^{86}Sr$ systematics of the granitoids indicates that this Hadean material is overall volumetrically of minor significance. As indicated by previous studies (Chaudhuri et al., 2018; Ranjan et al., 2020b), the well-defined trend of $^{176}Hf/^{177}Hf$ in zircon grains with progressively more negative εHf_i (pink and yellow evolution lines Fig. 7b) indicates that intra-crustal reworking of this earliest crustal material produced episodically younger, more evolved crust until 3.71 Ga. After that, a sudden shift has been reported (Chaudhuri et al., 2018; Ranjan et al., 2020b; Bauer et al., 2020) in the detrital and xenocrystic zircon Hf_i data, as the εHf_i values become more CHUR or DM like (vertical arrow at 3.7 Ga in Fig. 7b and Fig. 10b). Such a sudden shift in εHf_i values in zircons have been found in a number of other Archean cratons as well. Previous studies (Næraa et al., 2012; Bauer et al., 2020; Ranjan et al., 2020b) have concluded this discontinuity in εHf is the result of mixing of material derived from evolved crust (highly negative εHf_i) and juvenile mantle-derived (supra-chondritic to chondritic εHf_i) material. In the different Archean cratons, including the Singhbhum Craton, where the sudden shift in εHf_i have been documented so far, this shift has also been shown to correlate with marked changes in trace- and REE elemental ratios, particularly Nb/Th, U/Nb and Sc/Yb in zircon (Ranjan et al., 2020b; Drabon et al., 2022). The shift in $\delta^{49}Ti$ in granitoids from Acasta is contemporaneous with the shift in εHf_i in the same rocks (Aarons et al., 2020; Bauer et al., 2020). This type of shift in zircon εHf_i in combination with a shift in elemental ratios and variations in $\delta^{49}Ti$ indicates a fundamental change in style of felsic crust formation. As indicated by Reimink et al. (2019), Ranjan et al. (2020b), Bauer et al. (2020), Aarons et al. (2020), Drabon et al. (2022), the pronounced shift likely suggests change in granitoid formation from primarily shallow level crustal reworking of long-lived Hadean mafic crust in a dry Iceland-like intra-plate ocean plateau setting to granitoid formation from wet calc-alkaline precursors or from precursors produced by mixing of hydrous melts of subducted juvenile crust and older reworked material. However, Chowdhury et al. (2021) suggested formation of the older and younger granitoids in a plateau-like setting by melting of amphibolites at depth corresponding to pressure between 0.9 GPa and 1.2 GPa, in a non-plate tectonic regime. As indicated by Moyen (2011), in a pure plateau heating model for felsic crust formation, melting happens outside the stability field of garnet. Multiple studies (Pandey et al., 2019; Mitra et al., 2019; Upadhyay et al., 2019; Dey et al., 2019) using trace element signatures have shown that the parental magmas for Singhbhum TTGs and granites were derived from a rutile free, garnet and amphibole bearing source at depth corresponding to a pressure of 10–15 kbar. Furthermore, recent experimental work on production of TTGs (Hastie et al., 2023) has also shown that it is not possible to generate TTG magmas by heating the bottom section of a thick mafic plateau. Rather, subduction of hydrated basalt is required to produce TTG melts from an eclogite lithology. Hence, a transitional non-unique setting (Moyen, 2011) is needed to explain the TTG formation in the Singhbhum Craton (Upadhyay et al., 2019), where melts derived from recycled hydrated mafic crust facilitated the formation of the older granitoids (TTGs of Champua Suite) (Fig. 10c). Irrespective of the tectonic scenario, the timing of the sudden depleted mantle derived juvenile material input in the Singhbhum Craton at ~3.71 Ga (Fig. 7b) correlates with the extraction age (Hf model ages 3.77–3.65 Ga) of the mafic precursor for the Paleoarchean Singhbhum granitoids (Fig. 7a & b). This correlation links the modelled mafic precursor extraction with an actual mafic crust formation event recorded in the evolution history of the craton. This juvenile mafic crust sourced from the depleted mantle between 3.77 Ga and 3.65 Ga would have had the required $^{176}Lu/^{177}Hf$ (~0.020–0.025) and Rb/Sr (~0.0462–0.0615) to evolve for ~300 Ma and act as the primary precursor for older granitoids in the Singhbhum Craton (Fig. 10c).

Within the next 200 Ma, melts formed from residual older mafic crust (Fig. 10d) interacted with older granitoids (~3.53–3.44 Ga Champua Suit) and produced the younger granitoids (~3.4–3.2 Ga granites of Singhbhum Suite). This last episode of significant production of evolved felsic rocks was followed by the final stabilization of the Singhbhum Craton at 3.1–3.2 Ga (Olierook et al., 2019; Chowdhury et al., 2021; Chaudhuri et al., 2022), marked by the emplacement of late stage potassic granites of Mayurbhanj Suite (Hofmann et al., 2022). Beginning of voluminous granitoid production at ~3.53 Ga and continuation up to 3.1 Ga in the Singhbhum Craton also coincides with formation of extensive continental crust globally, as recorded in the Acasta gneiss complex of the Slave Craton (Bauer et al., 2017), Kapvaal Craton (Poujol et al., 2003), Pilbara Craton (Van Kranendonk et al., 2007) and the cratons of the Indian subcontinent, i.e. Western Dharwar Craton (Ranjan et al., 2020a), Bastar Craton (Maltese et al., 2021) and Bundelkhand craton (Singh et al., 2021).

6. Conclusions

The rapidly evolving Rb-Sr isotope system, particularly the $^{87}Sr/^{86}Sr_i$ directly determined in low Rb/Sr apatite, is very sensitive to magma differentiation and crustal extraction events. Consequently, Rb-Sr isotope system has high temporal resolution in identifying different precursor materials and their compositional evolution, even for precursors with short crustal residence time. Apatite in granitoids from the Singhbhum Craton is particularly suitable for obtaining initial Sr isotope compositions. Based on the whole rock-mica Rb-Sr isochron ages of the Singhbhum granitoids and paragneiss, it can be infered that the western part of the craton was not affected by any significant high-grade metamorphic overprinting after ~3.2 Ga. This puts the Singhbhum Craton in

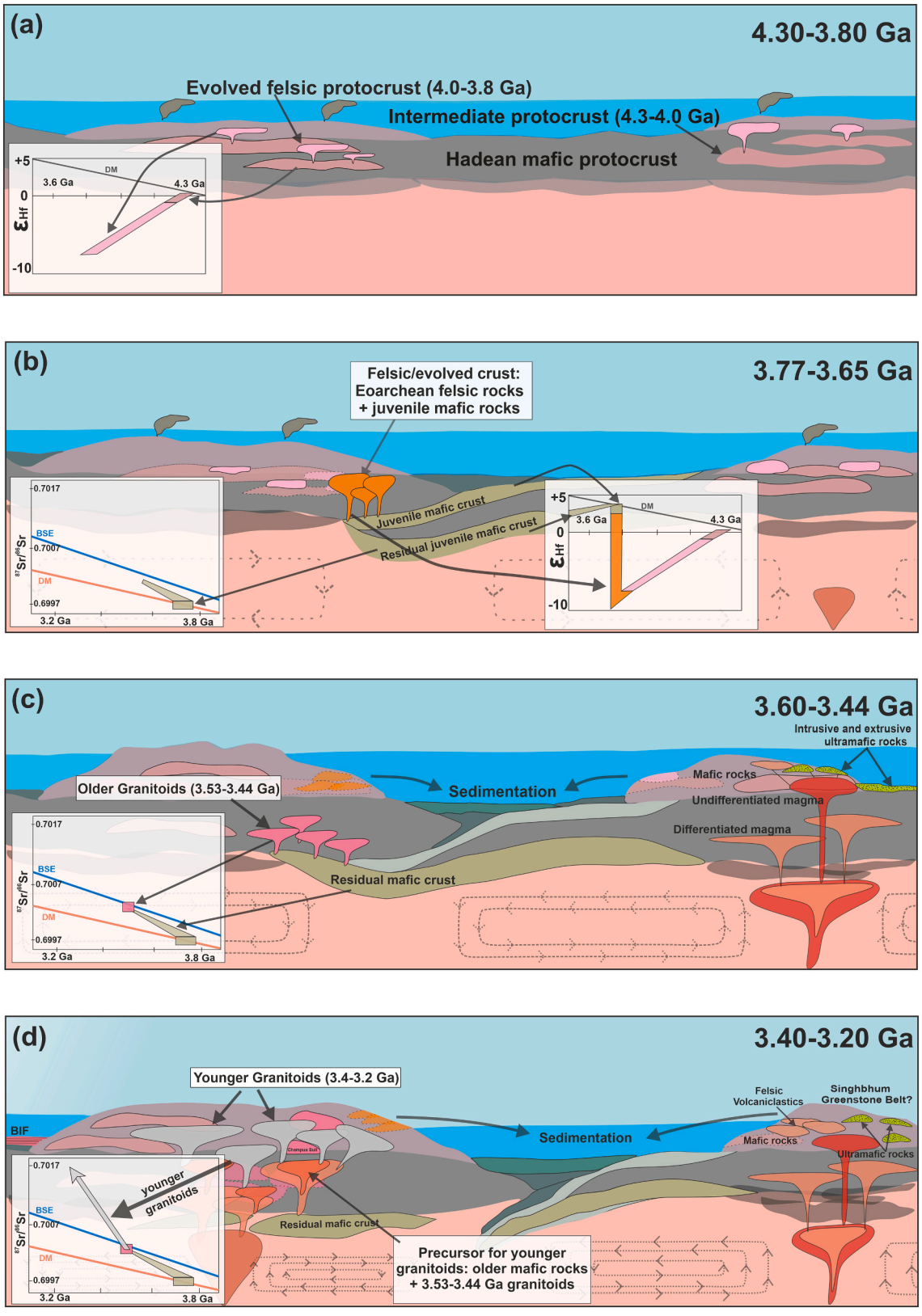

Fig. 10. Crustal evolution model for Singhbhum craton. Fig. a and b are adapted from Bauer et al. (2020). (a) Formation of Hadean mafic protocrust. Successive intra-crustal differentiation of mafic protocrust in a stagnant-lid setting formed intermediate and evolved proto-crustal units. (b) ~3.71 Ga, change from stagnant-lid to mobile-lid scenario. Input of depleted mantle derived juvenile mafic crust, which got recycled. Melt derived from recycled mafic crust interacted with the old evolved felsic material to form reworked felsic curst. Zircon grains from this felsic crust record the shift in εHf_i at ~3.71 Ga. (c) The residual portion of the mafic crust formed between 3.77 and 3.65 Ga evolved to become the precursor material for older granitoids (TTGs of Champua Suite) that formed between 3.53 and 3.44 Ga. (d) Subsequently, partial melts derived from the evolved and recycled mafic crust got mixed with partial melts generated from older granitoids to form the younger granitoids (granites of Singhbhum Suite).

a unique category of well-preserved Archean cratons, as most Archean cratonic blocks have seen multiple phases of high-grade metamorphic overprinting events which were commonly extended into the Proterozoic. This circumstance provides the opportunity to obtain close to initial Sr isotope compositions from apatite that did not recrystallize post-formation or soon after formation. Advancements in LA-MC-ICPMS analysis now allow precise in-situ measurement of Sr isotopes on single grains of apatite in the rock matrix or as inclusions (down to 20 μm) in zircon to obtain well-preserved $^{87}Sr/^{86}Sr_i$ from Paleoarchean rocks.

The combined isotope systematics of $^{87}Sr/^{86}Sr_i$ from apatite and Hf_i in whole rock and zircon of different felsic and meta-sedimentary rocks of the Singhbhum Craton, reveal a ~1 Ga history of crust extraction and differentiation that resulted in the formation of stable continental crust. As indicated by Hf isotopes in zircon, the Singhbhum Craton included minor amounts of mafic and differentiated crust of intermediate composition that formed as early as 4.4–4.25 Ga (Fig. 10a), and was reworked by later crust forming episodes. Subsequently, a new episode of crust formation was initiated by melt extraction from the depleted mantle, which produced juvenile mafic crust between 3.77 and 3.65 Ga. This period links the modelled extraction of the mafic precursor for the Paleoarchean granitoids in the Singhbhum Craton to an actual juvenile crust formation event recorded in the evolutionary history of the craton. Between 3.77 Ga and 3.65 Ga, felsic crust formed by assimilation of minor amounts of older felsic material with melts generated from juvenile mafic crust. Residual mafic crust sourced from the depleted mantle between 3.77 and 3.65 Ga evolved and became the source of the oldest phase of preserved granitoids (Champua Suite), which formed between 3.53 and 3.44 Ga. This process and its timing is documented by the primitive Sr isotope composition of apatite grains from the granitoids. Subsequent mixing of melts generated by partial melting of older granitoids (TTGs of Champua Suite) and melts formed by melting of older mafic rocks, generated the voluminous and mostly felsic younger granitoids (granites of Singhbhum Suite). Hence, three crust extraction and/or formation events at ~4.3–4.25 Ga, 3.77–3.65 Ga and 3.53–3.44 Ga (blue vertical bars in Fig. 7) contributed to the growth of felsic continental crust. With some crustal residence time, these crustal materials got evolved (orange vertical bars in Fig. 7). This was followed by partial reworking and mixing of the older crust with other juvenile or reworked materials to produce different younger generations of felsic crust, the most significant of which are the voluminous younger granitoids that were emplaced between 3.4 and 3.2 Ga in the Singhbhum Craton. This petrogenesis of Archean felsic crust in the Singhbhum Craton is consistent with a plate tectonic-like scenario which involves production of mafic crust (ocean floor) that was partially reworked in the garnet stability field (subducted mafic crust) and produced LREE enriched granitoids that now dominate the craton.

Declaration of Competing Interest

The authors declare that they have no known competing financial interests or personal relationships that could have appeared to influence the work reported in this paper.

Data availability

All the data can be found in the manuscript and supplementary materials.

Acknowledgement

Financial support for this study was provided by Swiss National Science Foundation grant (SNF grant no. 188592). The MC-ICP-MS at the Institute of Geological Sciences, University of Bern, used in this study was acquired within the framework of the NCCR project PlanetS (grant nr. 51NF40- 141881). NordSIMS-Vegacenter is funded by the Swedish Research Council as a national research infrastructure (dnr. 2021-00276). This is Vegacenter publication #069. SC extends his thanks to Alessandro Maltese for his help in measuring Rb - Sr isotopes in mica. SC is also thankful to Johannes Hämmerli for his help during apatite sample preparation and to Dewashish Upadhyay for guidance in the field and many fruitful discussions on Archean TTGs. We thank J. Jodder and one anonymous reviewer for their constructive and thorough comments that helped to improve the manuscript significantly. We also thank Sonja Aulbach for careful and efficient editorial handling of the manuscript.

Appendix A. Supplementary data

Two supplementary files are associated with this study. Supplementary file-1 is a pdf which has supplementary text and Supplementary Fig. 1 to 6. Supplementary file-2 is an EXCEL file which consists of supplementary data tables ST-1 to ST-6 (ST = Supplementary Table) in different sheets in the same file. Supplementary data to this article can be found online at https://doi.org/10.1016/j.chemgeo.2023.121772.

References

Aarons, S.M., Reimink, J.R., Greber, N.D., Heard, A.W., Zhang, Z., Dauphas, N., 2020. Titanium isotopes constrain a magmatic transition at the Hadean-Archean boundary in the Acasta Gneiss complex. Sci. Adv. 6 (50), 1–9.

Acharyya, S.K., Gupta, A., Orihashi, Y., 2010. Neoarchean-Paleoproterozoic stratigraphy of the Dhanjori basin, Singhbhum Craton, Eastern India: and recording of a few U-Pb zircon dates from its basal part. J. Asian Earth Sci. 39 (6), 527–536.

Amelin, Y., Lee, D., Halliday, A.N., Pidgeon, R.T., Hills, J., 1999. Nature of the Earth's earliest crust from hafnium isotopes in single detrital zircons. Nature 399 (6733), 252–255.

Antoine, C., Bruand, E., Guitreau, M., Devidal, J.L., 2020. Understanding preservation of primary signatures in apatite by comparing matrix and zircon-hosted crystals from the Eoarchean Acasta Gneiss complex (Canada). Geochem. Geophys. Geosyst. 21 (7) e2020GC008923.

Apen, F.E., Wall, C.J., Cottle, J.M., Schmitz, M.D., Kylander-Clark, A.R.C., Seward, G.G. E., 2022. Apatites for destruction: Reference apatites from Morocco and Brazil for U-Pb petrochronology and Nd and Sr isotope geochemistry. Chem. Geol. 590, 120689.

Bauer, A.M., Fisher, C.M., Vervoort, J.D., Bowring, S.A., 2017. Coupled zircon Lu–Hf and U–Pb isotopic analyses of the oldest terrestrial crust, the >4.03 Ga Acasta Gneiss Complex. Earth Planet. Sci. Lett. 458, 37–48.

Bauer, A.B., Reimink, J.R., Chacko, T., Foley, B.J., Shirey, S.B., Pearson, D.G., 2020. Hafnium isotopes in zircons document the gradual onset of mobile-lid tectonics. Geochem. Perspect. Lett. 14, 1–6.

Boehnke, P., Bell, E.A., Stephan, T., Trappitsch, R., Keller, C.B., Pardo, O.S., 2018. Potassic, high-silica Hadean crust. Proc. Natl. Acad. Sci. 115 (25), 6353–6356.

Bose, S., Ghosh, G., Kawaguchi, K., Das, K., Mondal, A.K., Banerjee, A., 2021. Zircon and monazite geochronology from the Rengali-Eastern Ghats Province: implications for the tectonic evolution of the eastern Indian terrane. Precambrian Res. 355, 106080.

Bouvier, A., Vervoort, J.D., Patchett, P.J., 2008. The Lu-Hf and Sm-Nd isotopic composition of CHUR: constraints from unequilibrated chondrites and implications for the bulk composition of terrestrial planets. Earth Planet. Sci. Lett. 273 (1–2), 48–57.

Bruand, E., Storey, C., Fowler, M., 2016. An apatite for progress: inclusions in zircon and titanite constrain petrogenesis and provenance. Geology 44 (2), 91–94.

Carlson, R.W., Lugmair, G.W., 1988. The age of ferroan anorthosite 60025: oldest crust on a young Moon? Earth Planet. Sci. Lett. 90, 119–130.

Caton, S.A., Smit, M.A., Emo, R.B., Musiyachenko, K.A., Kielman-Schmitt, M., Kooijman, E., Scherstén, A., Halla, J., Bleeker, W., Hoffmann, J.E., Pandey, O.P., Ravindran, A., Maltese, A., Mezger, K., 2022. Evolution of the sources of TTG and associated rocks during the Archean from in-situ $^{87}Sr/^{86}Sr$ isotope analysis of apatite by LA-MC-ICPMS. Lithos 428–429.

Cawood, P.A., Hawkesworth, C.J., Pisarevsky, S.A., Dhuime, B., Capitanio, F.A., Nebel, O., 2018. Geological archive of the onset of plate tectonics. Philos. Trans. R. Soc. A Math. Phys. Eng. Sci. 376 (2132), 20170405.

Chaudhuri, T., 2020. A review of Hadean to Neoarchean crust generation in the Singhbhum Craton, India and possible connection with Pilbara Craton, Australia: the geochronological perspective. Earth Sci. Rev. 202, 103085.

Chaudhuri, T., Wan, Y., Mazumder, R., Ma, M., Liu, D., 2018. Evidence of enriched, Hadean mantle reservoir from 4.2-4.0 Ga zircon xenocrysts from Paleoarchean TTGs of the Singhbhum Craton, Eastern India. Sci. Rep. 8 (1), 1–12.

Chaudhuri, T., Kamei, A., Das, M., Mazumder, R., Owada, M., 2022. Evolution of the Archean felsic crust of Singhbhum Craton, India: A reassessment. Earth Sci. Rev. 231, 104067.

Cherniak, D.J., 2000. Rare earth element diffusion in apatite. Geochim. Cosmochim. Acta 64 (22), 3871–3885.

Cherniak, D.J., Ryerson, F.J., 1993. A study of strontium diffusion in apatite using Rutherford backscattering spectroscopy and ion implantation. Geochim. Cosmochim. Acta 57 (19), 4653–4662.

Chowdhury, P., Gerya, T., Chakraborty, S., 2017. Emergence of silicic continents as the lower crust peels off on a hot plate-tectonic Earth. Nat. Geosci. 10, 698–703.

Chowdhury, P., Mulder, J.A., Cawood, P.A., Bhattacharjee, S., Roy, S., Wainwright, A.N., Nebel, O., Mukherjee, S., 2021. Magmatic thickening of crust in non–plate tectonic settings initiated the subaerial rise of Earth's first continents 3.3 to 3.2 billion years ago. Proc. Natl. Acad. Sci. 118 (46).
Conrad, C.P., Lithgow-Bertelloni, C., 2002. How mantle slabs drive plate tectonics. Science 298 (5591), 207–209.
Dey, S., Topno, A., Liu, Y., Zong, K., 2017. Generation and evolution of Palaeoarchaean continental crust in the central part of the Singhbhum craton, eastern India. Precambrian Res. 298, 268–291.
Dey, S., Mitra, A., Nandy, J., Mondal, S., Topno, A., Liu, Y., Zong, K., 2019. Early crustal evolution as recorded in the granitoids of the Singhbhum and Western Dharwar Cratons. Earth's Old. Rocks 1, 741–792.
Dhuime, B., Wuestefeld, A., Hawkesworth, C.J., 2015. Emergence of modern continental crust about 3 billion years ago. Nat. Geosci. 8 (7), 552–555.
Drabon, N., Byerly, B.L., Byerly, G.R., Wooden, J.L., Wiedenbeck, M., Valley, J.W., Kitajima, K., Bauer, A.M., Lowe, D.R., 2022. Destabilization of long-lived Hadean protocrust and the onset of pervasive hydrous melting at 3.8 Ga. AGU Adv. 3 (2).
Emo, R.B., Smit, M.A., Schmitt, M., Kooijman, E., Scherer, E.E., Sprung, P., Bleeker, W., Mezger, K., 2018. Evidence for evolved Hadean crust from Sr isotopes in apatite within Eoarchean zircon from the Acasta Gneiss complex. Geochim. Cosmochim. Acta 235, 450–462.
Frimmel, H.E., Chakravarti, R., Basei, M.A.S., 2022. Detrital zircon ages from Archaean conglomerates in the Singhbhum Craton, eastern India: implications on economic Au - U potential. Mineral. Deposita 57 (8), 1499–1514.
Ghosh, G., Bose, S., 2020. Deformation and metamorphic history of the Singhbhum Craton vis-a-vis peripheral mobile belts, eastern India: implications on Precambrian crustal processes. J. Mineral. Petrol. Sci. 115 (2), 70–87.
Gillespie, J., Kinny, P.D., Kirkland, C.L., Martin, L., Nemchin, A.A., Cavosie, A.J., Hasterok, D., 2021a. Isotopic modelling of Archean crustal evolution from comagmatic zircon–apatite pairs. Earth Planet. Sci. Lett. 575, 117194.
Gillespie, J., Nemchin, A.A., Kinny, P.D., Martin, L., Aleshin, M., Roberts, M.P., Ireland, T.R., Whitehouse, M.J., Jeon, H., Cavosie, A.J., Kirkland, C.L., 2021b. Strontium isotope analysis of apatite via SIMS. Chem. Geol. 559, 119979.
Giuliani, A., Jackson, M.G., Fitzpayne, A., Dalton, H., 2020. Remnants of early Earth differentiation in the deepest mantle-derived lavas. Proc. Natl. Acad. Sci. U. S. A. 118 (1), 1–9.
Goswami, J.N., Mishra, S., Wiedenbeck, M., Ray, S.L., Saha, A.K., 1995. 3.55Ga old zircon from Singhbhum-Orissa iron ore Craton, Eastern India. Curr. Sci. 69, 1008–1011.
Griffin, W.L., Pearson, N.J., Belousova, E., Jackson, S.E., van Achterbergh, E., O'Reilly, S. Y., Shee, S.R., 2000. The Hf isotope composition of cratonic mantle: LAM-MC-ICPMS analysis of zircon megacrysts in kimberlites. Geochim. Cosmochim. Acta 64 (1), 133–147.
Hastie, A.R., Law, S., Bromiley, G.D., Fitton, J.G., Harley, S.L., Muir, D.D., 2023. Deep formation of Earth's earliest continental crust consistent with subduction. Nat 16, 816–821.
Hofmann, A., Jodder, J., Xie, H., Bolhar, R., Whitehouse, M., Elburg, M., 2022. The Archaean geological history of the Singhbhum Craton, India–a proposal for a consistent framework of craton evolution. Earth Sci. Rev. 228, 103994.
Horstwood, M.S.A., Evans, J.A., Montgomery, J., 2008. Determination of Sr isotopes in calcium phosphates using laser ablation inductively coupled plasma mass spectrometry and their application to archaeological tooth enamel. Geochim. Cosmochim. Acta 72, 5659–5674.
Jagoutz, O., Kelemen, P.B., 2015. Role of arc processes in the formation of continental crust. Annu. Rev. Earth Planet. Sci. 43, 363–404.
Jeon, H., Whitehouse, M.J., 2021. A Robust LG-SIMS method for Sr isotope determination in apatite across a wide Sr concentration range. Geostand. Geoanal. Res. 45 (2), 325–340.
Jodder, J., Hofmann, A., Ueckermann, H., 2021. 3.51 Ga old felsic volcanic rocks and carbonaceous cherts from the Gorumahisani Greenstone Belt – insights into the Palaeoarchaean record of the Singhbhum Craton, India. Precambrian Res. 357, 106109.
Jodder, J., Hofmann, A., Xie, H., Elburg, M.A., Wilson, A., 2023. Geochronology of the Daitari Greenstone Belt, Singhbhum Craton, India. Precambrian Res. 388, 106997.
Kooijman, E., Mezger, K., Berndt, J., 2010. Constraints on the U–Pb systematics of metamorphic rutile from in situ LA-ICP-MS analysis. Earth Planet. Sci. Lett. 293 (3–4), 321–330.
Kröner, A., Elis Hoffmann, J., Xie, H., Wu, F., Münker, C., Hegner, E., Wong, J., Wan, Y., Liu, D., 2013. Generation of early Archaean felsic greenstone volcanic rocks through crustal melting in the Kaapvaal, craton, southern Africa. Earth Planet. Sci. Lett. 381, 188–197.
Maltese, A., Mezger, K., Upadhyay, D., Berndt, J., Scherer, E.E., 2021. On the petrogenesis of Paleoarchean continental crust: U-Pb-Hf isotope and major-trace element constraints from the Bastar Craton, India. Chem. Geol. 579, 120337.
Maltese, A., Caro, G., Pandey, O.P., Upadhyay, D., Mezger, K., 2022. Direct evidence for crust-mantle differentiation in the late Hadean. Commun. Earth Environ. 3 (1), 1–6.
McDonough, W.F., Sun, S., 1995. The composition of the Earth. Chem. Geol. 120 (3–4), 223–253.
Mezger, K., Hanson, G.N., Bohlen, S.R., 1989. High-precision UPb ages of metamorphic rutile: application to the cooling history of high-grade terranes. Earth Planet. Sci. Lett. 96 (1–2), 106–118.
Mezger, K., Maltese, A., Vollstaedt, H., 2021. Accretion and differentiation of early planetary bodies as recorded in the composition of the silicate Earth. Icarus 365, 114497.
Miller, S.R., Mueller, P.A., Meert, J.G., Kamenov, G.D., Pivarunas, A.F., Sinha, A.K., Pandit, M.K., 2018. Detrital zircons reveal evidence of Hadean crust in the Singhbhum Craton, India. J. Geol. 126 (5), 541–552.
Mishra, S., Deomurari, M.P., Wiedenbeck, M., Goswami, J.N., Ray, S., Saha, A.K., 1999. $^{207}Pb/^{206}Pb$ zircon ages and the evolution of the Singhbhum Craton, eastern India: an ion microprobe study. Precambrian Res. 93 (2–3), 139–151.
Mitra, A., Dey, S., Zong, K., Liu, Y., Mitra, A., 2019. Building the core of a Paleoarchean continent: evidence from granitoids of Singhbhum Craton, eastern India. Precambrian Res. 335, 105436.
Mitra, Aniruddha, Dey, S., Das, P., Zong, K., Liu, Y., Mitra, Anirban, Gond, A.K., 2022. Time-space evolution of an ancient continent, a window to changing crustal architecture: insights from granitoids of Singhbhum Craton, eastern India. Earth Sci. Rev. 234, 104183.
Moorbath, S., Taylor, P.N., Jones, N.W., 1986. Dating the oldest terrestrial rocks - fact and fiction. Chem. Geol. 57 (1–2), 63–86.
Moore, W.B., Webb, A.A.G., 2013. Heat-pipe Earth. Nature 501, 501–505.
Moyen, J.F., 2011. The composite Archaean grey gneisses: petrological significance, and evidence for a non-unique tectonic setting for Archaean crustal growth. Lithos 123 (1–4), 21–36.
Moyen, J.-F., Laurent, O., 2018. Archaean tectonic systems: a view from igneous rocks. Lithos 302–303, 99–125.
Mukhopadhyay, D., Matin, A., 2020. The architecture and evolution of the Singhbhum Craton. Episodes 43 (1), 19–50.
Mukhopadhyay, J., Beukes, N.J., Armstrong, R.A., Zimmermann, U., Ghosh, G., Medda, R.A., 2008. Dating the oldest greenstone in India: A 3.51-Ga precise U-Pb SHRIMP zircon age for dacitic lava of the southern Iron Ore Group, Singhbhum Craton. J. Geol. 116, 449–461.
Næraa, T., Scherstén, A., Rosing, M.T., Kemp, A.I.S., Hoffmann, J.E., Kokfelt, T.F., Whitehouse, M.J., 2012. Hafnium isotope evidence for a transition in the dynamics of continental growth 3.2Gyr ago. Nature 485 (7400), 627–630.
Nebel, O., Scherer, E.E., Mezger, K., 2011. Evaluation of the ^{87}Rb decay constant by age comparison against the U–Pb system. Earth Planet. Sci. Lett. 301 (1–2), 1–8.
Olierook, H.K., Clark, C., Reddy, S.M., Mazumder, R., Jourdan, F., Evans, N.J., 2019. Evolution of the Singhbhum Craton and supracrustal provinces from age, isotopic and chemical constraints. Earth Sci. Rev. 193, 237–259.
O'Neil, J., Carlson, R.W., 2017. Building Archean cratons from Hadean mafic crust. Science 355 (6330), 1199–1202.
Page, R.W., Bell, T.H., 1986. Isotopic and structural responses of granite to successive deformation and metamorphism (Australia). J. Geol. 94 (3), 365–379.
Pandey, O.P., Mezger, K., Ranjan, S., Upadhyay, D., Villa, I.M., Nägler, T.F., Vollstaedt, H., 2019. Genesis of the Singhbhum Craton, eastern India; implications for Archean crust-mantle evolution of the Earth. Chem. Geol. 512, 85–106.
Poujol, M., Robb, L.J., Anhaeusser, C.R., Gericke, B., 2003. A review of the geochronological constraints on the evolution of the Kaapvaal Craton, South Africa. Precambrian Res. 127 (1–3), 181–213.
Prabhakar, N., Bhattacharya, A., 2013. Paleoarchean partial convective overturn in the Singhbhum Craton, Eastern India. Precambrian Res. 231, 106–121.
Raczek, I., Jochum, K.P., Hofmann, A.W., 2003. Neodymium and strontium isotope data for USGS reference materials BCR-1, BCR -2, BHV O-1, BHVO-2, AGV-1, AGV-2, GSP-1, GSP-2 and Eight MPI-DING reference glasses. Geostand. Newslett. 27, 173–179.
Ranjan, S., Upadhyay, D., Abhinay, K., Srikantappa, C., 2020a. Paleoarchean and Neoarchean Tonalite–Trondhjemite–Granodiorite (TTG) and granite magmatism in the Western Dharwar Craton, southern India: implications for Archean continental growth and geodynamics. Precambrian Res. 340, 105630.
Ranjan, S., Upadhyay, D., Lochan, K., Nanda, J.K., 2020b. Detrital zircon evidence for change in geodynamic regime of continental crust formation 3.7 – 3.6 billion years ago. Earth Planet. Sci. Lett. 538, 116206.
Ravindran, A., Mezger, K., Balakrishnan, S., Kooijman, E., Schmitt, M., Berndt, J., 2020. Initial 87 Sr / 86 Sr as a sensitive tracer of Archaean crust-mantle evolution: constraints from igneous and sedimentary rocks in the western Dharwar. Precambrian Res. 337, 105523.
Reimink, J.R., Pearson, D.G., Shirey, S.B., Carlson, R.W., Ketchum, J.W.F., 2019. Onset of new, progressive crustal growth in the central Slave craton at 3.55 Ga. Geochem. Perspect. Lett. 10, 8–13.
Saha, A.K., 1994. Crustal evolution of Singhbhum-North Orissa, Eastern India. 27 Geological Society of India, Memoir (341 pp).
Sano, Y., Terada, K., Hidaka, H., Yokoyama, K., Nutman, A.P., 1999. Palaeoproterozoic thermal events recorded in the ~4.0Ga Acasta gneiss, Canada: evidence from SHRIMP U-Pb dating of apatite and zircon. Geochim. Cosmochim. Acta 63 (6), 899–905.
Scherer, E., Munker, C., Mezger, K., 2001. Calibration of the lutetium-hafnium clock. Science 293 (5530), 683–687.
Sharma, M., Basu, A.R., Ray, S.L., 1994. Sm-Nd isotopic and geochemical study of the Archean tonalite-amphibolite association from the eastern Indian Craton. Contrib. Mineral. Petrol. 117 (1), 45–55.
Singh, P.K., Verma, S.K., Singh, V.K., Moreno, J.A., Oliveira, E.P., Li, X.H., Malviya, V.P., Prakash, D., 2021. Geochronology and petrogenesis of the TTG gneisses and granitoids from the Central Bundelkhand granite-greenstone terrane, Bundelkhand Craton, India: implications for Archean crustal evolution and cratonization. Precambrian Res. 359, 106210.
Sizova, E., Gerya, T., Stüwe, K., Brown, M., 2015. Generation of felsic crust in the Archean: a geodynamic modeling perspective. Precambrian Res. 271, 198–224.
Sreenivas, B., Dey, S., Bhaskar Rao, Y.J., Vijaya Kumar, T., Babu, E.V.S.S.K., Williams, I. S., 2019. A new cache of Eoarchaean detrital zircons from the Singhbhum craton, eastern India and constraints on early Earth geodynamics. Geosci. Front. 10 (4), 1359–1370.

Stern, R.J., 2018. The evolution of plate tectonics. Philos. Trans. R. Soc. A Math. Phys. Eng. Sci. 376.
Stracke, A., Scherer, E.E., Reynolds, B.C., 2013. Application of isotope dilution in geochemistry. In: Treatise on Geochemistry, , Second editionVol. 15. Elsevier Ltd.
Upadhyay, D., Chattopadhyay, S., Kooijman, E., Mezger, K., Berndt, J., 2014. Magmatic and metamorphic history of Paleoarchean tonalite-trondhjemite-granodiorite (TTG) suite from the Singhbhum craton, eastern India. Precambrian Res. 252, 180.
Upadhyay, D., Chattopadhyay, S., Mezger, K., 2019. Formation of Paleoarchean-Mesoarchean Na-rich (TTG) and K-rich granitoid crust of the Singhbhum craton, eastern India: constraints from major and trace element geochemistry and Sr-Nd-Hf isotope composition. Precambrian Res. 327, 255–272.
Van Kranendonk, M.J., Hugh Smithies, R., Hickman, A.H., Champion, D.C., 2007. Secular tectonic evolution of Archean continental crust: interplay between horizontal and vertical processes in the formation of the Pilbara Craton, Australia. Terra Nova 19 (1), 1–38.
Vezinet, A., Pearson, D.G., Thomassot, E., Stern, R.A., Sarkar, C., Luo, Y., Fisher, C.M., 2018. Hydrothermally-altered mafic crust as source for early Earth TTG: Pb/Hf/O isotope and trace element evidence in zircon from TTG of the Eoarchean Saglek Block, N. Labrador. Earth Planet. Sci. Lett. 503, 95–107.
Vohra, C.P., Dasgupta, S., Paul, P.K., Bishui, P.K., Gupta, S.N., Guha, S., 1991. Rb-Sr chronology and petrochemistry of granitoids from the south-eastern part of the Singhbhum craton, Orissa. J. Geol. Soc. India 38 (1), 5–22.
Workman, R.K., Hart, S.R., 2005. Major and trace element composition of the depleted MORB mantle (DMM). Earth Planet. Sci. Lett. 231 (1–2), 53–72.
Yang, Y.H., Wu, F.Y., Yang, J.H., Chew, D.M., Xie, L.W., Chu, Z.Y., Zhang, Y., bin, & Huang, C., 2014. Sr and Nd isotopic compositions of apatite reference materials used in U-Th-Pb geochronology. Chem. Geol. 385, 35–55.